Journal of Asian Earth Sciences 57 (2012) 103–119

Contents lists available at SciVerse ScienceDirect

Journal of Asian Earth Sciences

journal homepage: www.elsevier.com/locate/jseaes

Evolution of the Bababurnu Basin and shelf of the Biga Peninsula: Western extension of the middle strand of the North Anatolian Fault Zone, Northeast Aegean Sea, Turkey

C. Yaltırak [a,*], E.B. İşler [b], A.E. Aksu [b], R.N. Hiscott [b]

[a] Istanbul Technical University, Faculty of Mines, Department of Geological Engineering, Ayazağa, Istanbul 34426, Turkey
[b] Department of Earth Sciences, Centre for Earth Resources Research, Memorial University of Newfoundland, St. John's, Newfoundland and Labrador, Canada A1B 3X5

ARTICLE INFO

Article history:
Received 5 February 2012
Received in revised form 18 June 2012
Accepted 25 June 2012
Available online 4 July 2012

Keywords:
North Anatolian Fault Zone
Northeast Aegean Sea
Tectonics
Pull-apart basin
Seismic stratigraphy

ABSTRACT

The generally transpressional character of the North Anatolian Fault Zone in western Turkey implies a transtensional character in the Northern Aegean Sea. The geological evolution of the basins lying above and immediately adjacent to this fault zone is still poorly understood. Similarly little information exists regarding the tectonic configurations created by the westerly and southerly extension of the middle and southern strands of the North Anatolian Fault Zone into the Northern Aegean Sea, other than what has been inferred using somewhat speculative maps onland. This study combines ~1600 km of single-channel seismic reflection profiles and piston-core data with detailed land mapping to develop a comprehensive evolutionary model. We suggest that the tectonic system of the Biga Peninsula and the northeastern Aegean Sea are characterized by transpressional broken-slat geometry onland and transtensional broken-slat geometry at sea. The system includes a set of prominent NE–SW-striking faults with considerable strike-slip component in the east (northwestern Turkey and eastern Aegean Sea) and a second set of major NW–SE-striking extensional faults in the west (eastern Greece). We further suggest that rotational wedges form the link between the NE–SW- and NW–SE-striking faults. Detailed mapping of the seismic data and fault linkages with the onland geology demonstrate that the middle strand of the North Anatolian Fault Zone exits into the Aegean Sea near the town of Behramkale and that it extends into the Bababurnu pull-apart basin in the northeastern Aegean Sea as a right-releasing step-over active during the Quaternary.

1. Introduction

The Aegean Sea and adjacent western Turkey and Greece form one of the most seismically active areas of the eastern Mediterranean (Fig. 1). Several previous studies have revealed the complexity of the region in terms of seismicity, fault kinematics, and structural evolution (Dewey and Şengör, 1979; Le Pichon and Angelier, 1979; Şengör, 1979; Şengör et al., 2005). At present, seismological data, earthquake fault-plane solutions, motions deduced from Global Positioning System (GPS) stations, and shallow reflection seismic data have shown that the northeastern Aegean region is under a transtensional stress regime (Taymaz et al., 1991; Reilinger et al., 1997; Kahle et al., 1998; Papazachos et al., 1998; Yaltırak et al., 1998; Yaltırak and Alpar, 2002b). GPS data clearly show the counterclockwise rotation of the Aegean–Anatolian Microplate, south of the North Anatolian Fault Zone, and the progressive west to southwest increase in the velocity of the microplate towards the Hellenic Arc (Fig. 1A Reilinger et al., 1997; McClusky et al., 2000). The western, Aegean segment of the microplate experiences intense normal-slip and dextral strike-slip faulting as indicated by fault-plane solutions of recent earthquakes (Fig. 1B; McKenzie, 1978; Taymaz et al., 1991; Papazachos et al., 1998) and regional structural maps (Fig. 1B; Mascle and Martin, 1990; Reilinger et al., 1997; Yaltırak et al., 1998; Papanikolaou et al., 2002; Yaltırak, 2002).

The most prominent depressions in the northern Aegean Sea are the North Aegean Trough, Saros Basin, North Skyros Basin and the Bababurnu Basin (Fig. 1B). Regional seismic reflection profiles show that the structural framework of the northern Aegean Sea is characterized by a series of NE–SW-striking major basin-bounding faults (Fig. 1B; Le Pichon and Angelier, 1979; Mascle and Martin, 1990; Saatçılar et al., 1999; Yaltırak and Alpar, 2002b). Regional seismicity and kinematic analyses of faults have shown that normal faulting and strike-slip faulting are the two dominant mechanisms controlling seabed morphology in the north Aegean Sea due to the complex interaction of crustal extension and slip along the North Anatolian Fault Zone (Kiratzi et al., 1991; Taymaz

* Corresponding author.
E-mail address: yaltirak@itu.edu.tr (C. Yaltırak).

1367-9120/$ - see front matter © 2012 Elsevier Ltd. All rights reserved.
http://dx.doi.org/10.1016/j.jseaes.2012.06.016

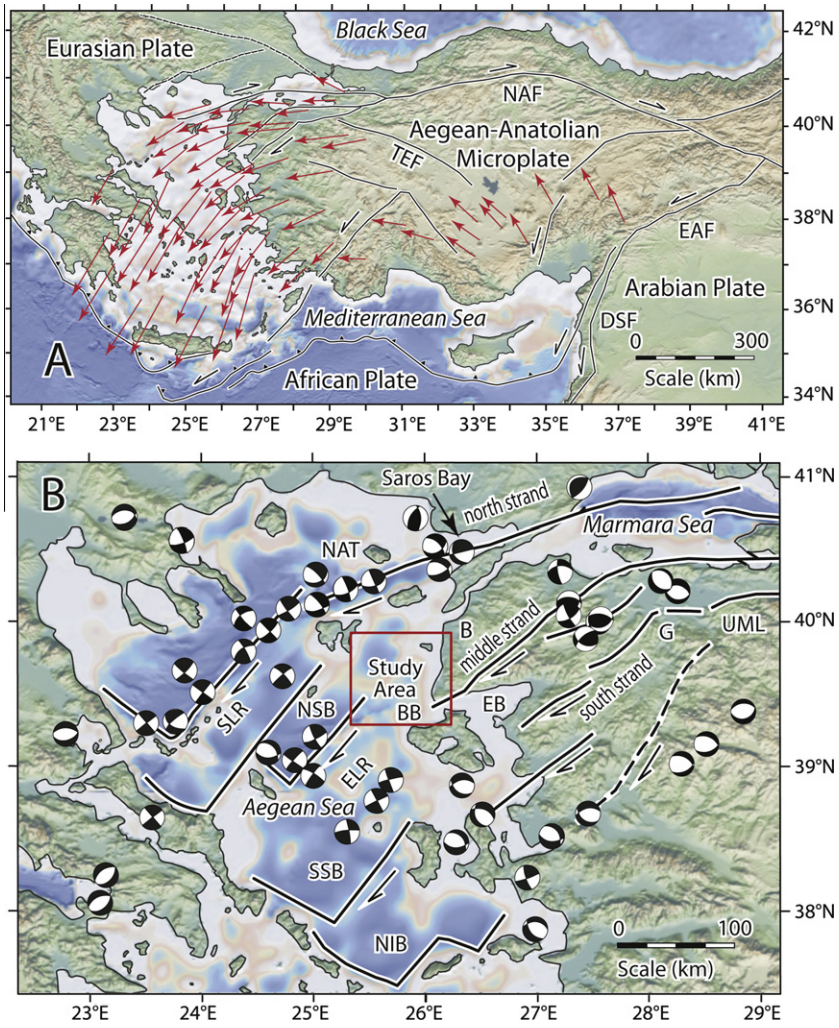

Fig. 1. (A) GPS vectors relative to a fixed Eurasian Plate showing the counterclockwise rotation of the Aegean–Anatolian Microplate (Reilinger et al., 1997). DSF: Dead Sea Fault Zone, EAF: East Anatolian Fault Zone, NAF: North Anatolian Fault Zone TEF: Thrace-Eskişehir Fault Zone. (B) Simplified tectonic map of the northern Aegean Sea showing the predominantly NE–SW-striking transtensional structures, compiled from Mascle and Martin (1990), Yaltırak et al. (1998), Papanikolaou et al. (2002) and Yaltırak (2002). Fault plane solutions are from McKenzie (1978), Taymaz et al. (1991) and Papazachos et al. (1998). B: Biga Peninsula, BB: Bababurnu Basin, EB: Edremit Bay, ELR: Euboea-Lesvos Ridge, G: Gönen, SB: Saros Basin, NAT: North Aegean Trough, NIB: North Ikaria Basin, NSB: North Sykros Basin, SLR: Sporades-Limnos Ridge, SSB: South Skyros Basin, UML: Ulubat and Manyas Lakes. Topography and bathymetry are from Digital Elevation Model using GeoMapApp data base (Ryan et al., 2009).

et al., 1991; Yaltırak et al., 1998; Saatçılar et al., 1999; Yaltırak and Alpar, 2002b).

Several researchers have only schematically illustrated the strands of the North Anatolian Fault Zone in the Aegean Sea, and in most cases land-based mapping have not been taken into account (Papadimitriou and Sykes, 2001; Meade et al., 2002; Papanikolaou and Papanikolaou, 2007). The study area for this paper encompasses a critical location where the middle strand of the North Anatolian Fault Zone crosses from the Turkish mainland and enters into the Aegean Sea (Fig. 1B). The aim of this study is (i) to delineate the Pliocene–Quaternary tectonic and kinematic framework of the northeastern Aegean Sea, (ii) to understand processes involved in the formation of basins in this region, and (iii) to establish first-order correlations between structures observed in northwestern Turkey and those mapped in the northern Aegean Sea.

2. Data acquisition and methods

During cruises in 1998, 2000, 2002 and 2003 (Memorial University of Newfoundland cruise numbers MAR98, MAR00, MAR02 and MAR03), ~1600 km of seismic reflection and side-scan sonar profiles were collected from the northeastern Aegean Sea, using the RV Koca Piri Reis of the Institute of Marine Sciences and Technol-

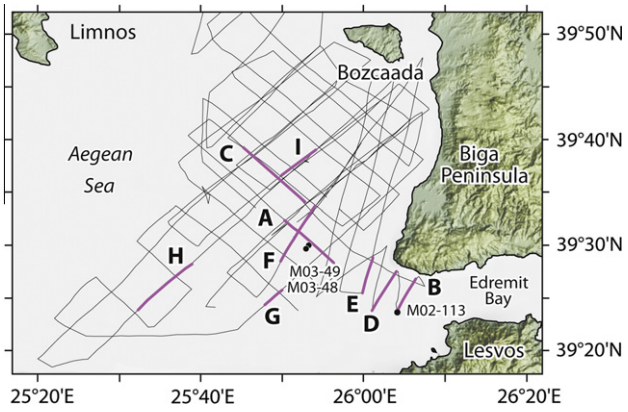

Fig. 2. Index map showing the study area and the location of seismic reflection profiles collected during the MAR98, MAR00, MAR02 and MAR03 cruises of the RV Koca Piri Reis. Circles denote piston core locations. Heavy lines A through I show seismic profiles illustrated in subsequent figures.

ogy, Izmir, Turkey (Fig. 2). All navigational fixes were determined using a GPS receiver. The bathymetry was recorded every 10 min using a 12 kHz echo-sounder collected along all the seismic reflection profiles shown in Fig. 2. A bathymetric map was constructed using the previously contoured maps (e.g., IOC, 1981) and the bathymetric data collected during the above cruises. In regions were additional data were needed, depth information was extracted from seismic reflection profiles using 1500 m/s velocities.

Huntec deep-tow system profiles were collected using a 0.5 kJ multi-tip sparker source (1998) or a 0.5 kJ boomer source (2000). Reflections were received using both a single high-resolution fish-mounted internal hydrophone and a fish-mounted 21-element, 6 m-long Benthos hydrophone streamer. In 1998, additional sparker profiles were collected using a 1.58 kJ multi-tip sparker source. During the 2000 and 2002 cruises, profiles were collected using a 40 cubic inch (655 cm^3) sleeve gun source, and two streamers: a 7.6 m-long Benthos Mesh 25/50P 50-element streamer and a 6.7 m-long 25-element Nova Scotia Research Foundation Corporation streamer. In 2000, side-scan sonar data were collected in conjunction with seismic reflection profiles using a Klein 590 system.

3. Bathymetry

The study area is located in the northeastern Aegean Sea, south of the Island of Bozcaada, north of the Island of Lesvos and west of the Biga Peninsula (Figs. 1B and 3). Across the shelf, the seabed has a smooth to gently undulating morphology with gradients ranging between 0.1° and 1.8°. The shelf break occurs at an average depth of −120 m. Seaward of the shelf, steep slopes (8–13°) lead to a deep basin (Bababurnu Basin) between the Biga Peninsula and the Island of Lesvos (Fig. 3). Across the southern fringes of the Biga Peninsula, the shelf is extremely narrow and very steep, and the elevation difference between coastal hills and the seafloor exceeds ~750 m (Fig. 3).

4. Geology

4.1. Biga Peninsula

The Biga Peninsula includes rocks ranging in age from Carboniferous to Tertiary, as well as unconsolidated Quaternary alluvium (Fig. 4; Yaltırak, 2003). Pre-Tertiary basement is covered by Eocene to Oligocene siliciclastic and volcanic successions (Siyako et al., 1989). Eocene granodiorites intrude the pre-Tertiary basement (Yılmaz and Karacık, 2001). Upper Oligocene – Lower Miocene granodiorites are associated with contemporaneous and consanguineous calc-alkaline volcanic and volcano-sedimentary successions. The volcanics are overlain by Lower Miocene terrigenous sediments capped by a Lower-Middle Miocene turbidite unit and lacustrine tuffs (Fig. 4).

In the western part of the Biga Peninsula, Upper Miocene marine limestones and lagoonal calcareous clastics display local unconformable relationships with the underlying volcanic rocks (Fig. 4; Sakınç and Yaltırak, 2005). Upper Miocene basalts are intercalated with the marine and lagoonal sediments. Miocene formations located around the northern shores of Edremit Bay are unconformably overlain by Upper Pliocene – Recent alluvial-fan deposits (Yaltırak, 2003). In the offshore Bababurnu Basin, a series of seismic units overlies equivalents of the Upper Pliocene – Recent alluvial fans and lacustrine deposits (İşler et al., 2008). These seismic units are interpreted as marine deposits of Pleistocene to Holocene age that accumulated during glacial and inter-glacial epochs (described below).

Immediately east of the study area and on the western Biga Peninsula (Fig. 4) basement rocks are overlain by Lower – Middle Miocene volcanic and volcano-sedimentary successions (Yılmaz and Karacık, 2001), in turn overlain by Middle – Upper Miocene marine and lagoonal sediments (Sakınç and Yaltırak, 2005), which are unconformably overlain by the Pliocene–Quaternary successions (Yaltırak et al., 2000b). In the Limnos-1 exploration well (Fig. 4) drilled west of Bozcaada on the Biga Shelf, a 330 m-thick Pliocene–Quaternary package overlies a 660 m-thick Miocene succession, which in turn overlies the Eocene basement (Lalechos and Savoyat, 1977). In the Kilitbahir-1 well on the Gelibolu Peninsula to the north of the study area, a ~1060 m-thick Miocene succession overlies the Eocene basement (Yaltırak and Alpar, 2002b). Although the Pliocene–Quaternary is not encountered in the Kilitbahir-1 well, the alluvial-fan deposits of the Conkbayırı Formation occur as a widespread veneer (up to 350 m thick) across the Gelibolu Peninsula, unconformably atop the Miocene sedimentary rocks (Yaltırak, 1995). In the Edremit-1 well drilled in Edremit Bay, a 585 m-thick Pliocene–Quaternary siliciclastic succession overlies first a 747 m-thick Upper – Middle Miocene sedimentary succes-

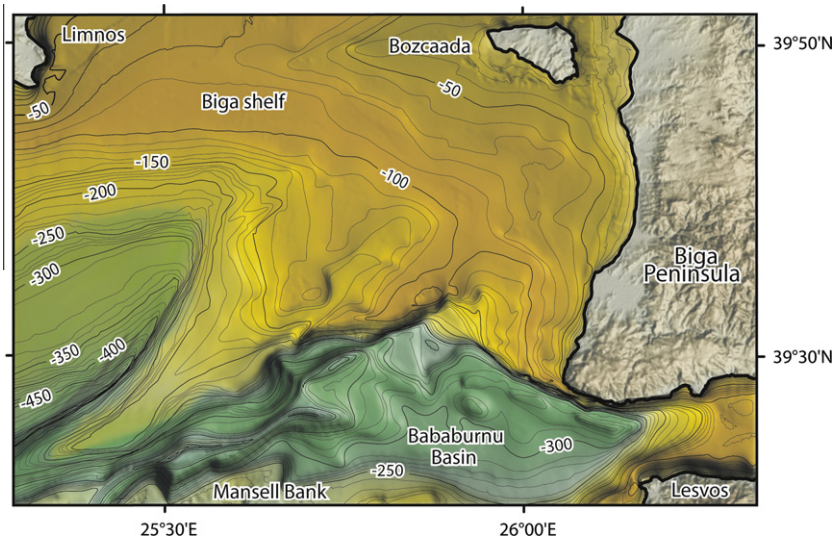

Fig. 3. Bathymetric map of the study area, compiled using soundings obtained during cruises of the RV K Piri Reis in 1998, 2000 and 2002 which are augmented by data from maps published by the IOC (1981). Isobaths are in metres.

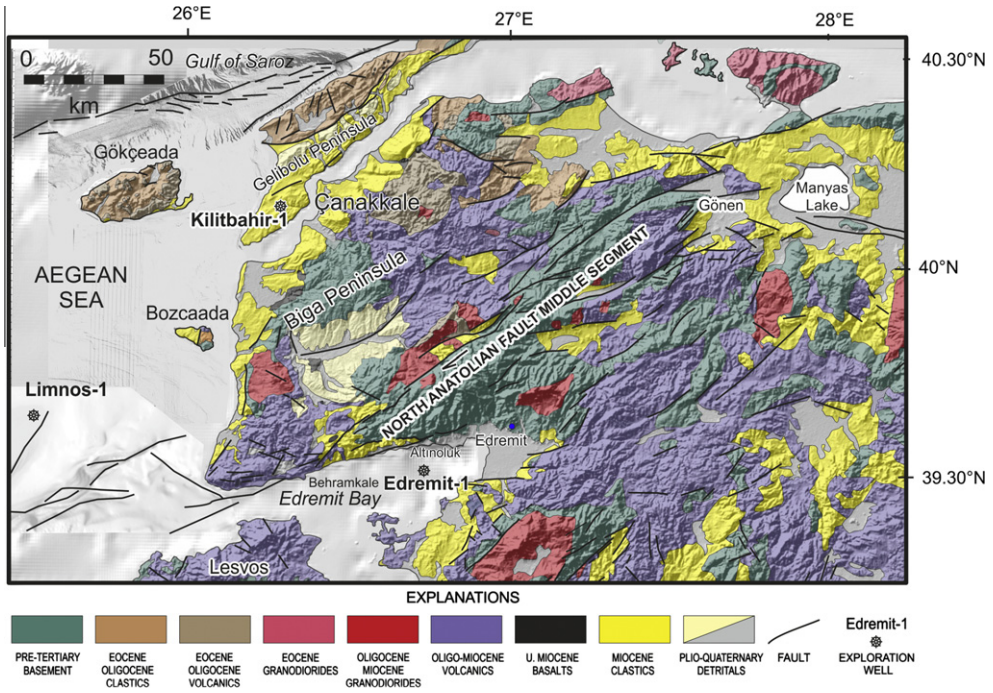

Fig. 4. Geological map of the Biga Peninsula, compiled from Altunkaynak and Yılmaz (1998), Genç (1998), Yaltırak et al. (1998), Yılmaz and Karacık (2001) and Yaltırak (2002, 2003). Also shown are large faults and exploration wells: Kilitbahir-1, Limnos-1 and Edremit-1. Gulf of Saroz faults and multibeam bathymetry compiled from Ustaömer et al. (2008).

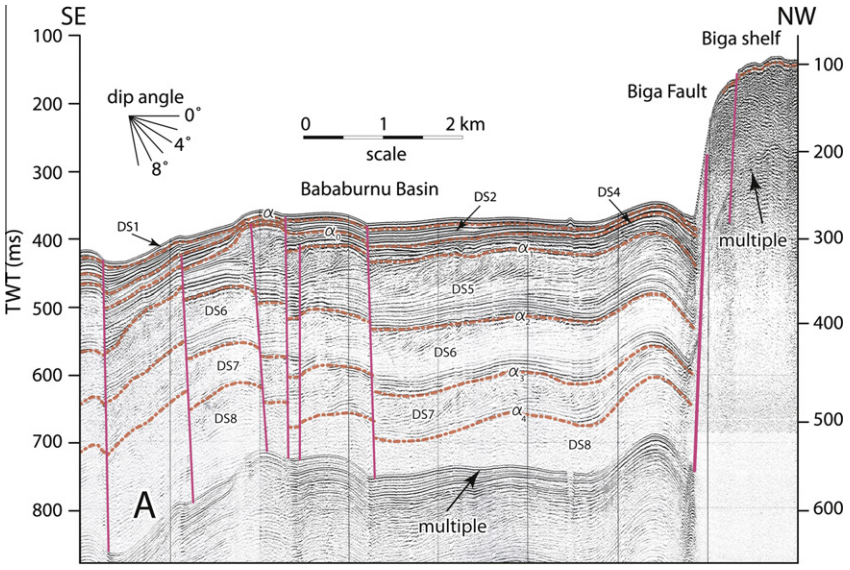

Fig. 5. Air-gun seismic reflection profile "**A**" showing the internal architecture of the stacked, prograded depositional sequences 5, 6, 7, 8, their bounding unconformities α, α_0, α_1, α_2, α_3, α_4, the distal reflections of depositional sequences (DS), and their bounding correlative conformities in deeper water regions in the Bababurnu Basin. Also shown are the Biga Fault and smaller faults that cuts these sequences (discussed in text). See Fig. 2 for location.

sion, then a >2200 m-thick Lower Miocene to Recent succession. Yaltırak (2003) described a Pliocene–Quaternary seismic unit having a maximum acoustic two-way travel time of 1.1 s (~1000 m) in nearby deep seismic lines. Along the northern shore of Edremit Bay, the Lower Miocene is ~700 m thick (Yaltırak, 2003). The above data show that 600–1600 m-thick Miocene volcanic and sedimentary successions are unconformably overlain by 300–1020 m of Pliocene–Quaternary strata over a wide area in and around Edremit Bay.

4.2. Offshore

On the basis of reflection configuration and internal architecture, several vertically stacked depositional sequences are delineated in the seismic reflection profiles collected from the offshore region adjacent to Biga Peninsula (Fig. 5; also see İşler et al., 2008). Each depositional sequence generally includes an upper subunit characterized by oblique to sigmoid-oblique clinoforms and a lower subunit characterized by continuous parallel

to sub-parallel reflectors (Fig. 5). The depositional sequences are separated from one another by prominent shelf-crossing unconformities, which developed by subaerial exposure and erosion that culminated at the time of the maximum regression, followed by shoreface erosion during the subsequent transgression when longshore currents and waves cut a ravinement surface (Fig. 5; İşler et al., 2008).

5. Chronostratigraphy of Biga Shelf and Bababurnu Basin

There are no long boreholes in the study area, so the dating of all but the youngest shelf-crossing unconformities depends on extrapolation of near-surface sedimentation rates into deeper strata and the application of constraints based on the principles of sequence stratigraphy. A basinal site beyond the seaward limit of sigmoid-oblique clinoforms (cf., (Mitchum et al., 1977) was selected for assessment of the chronology because of the good prospect of continuous deposition in deeper water where shelf-crossing unconformities have passed distally into correlative conformities (Helland-Hansen and Martinsen, 1996) Compaction is not significant at burial depths less than ~150 m so an average accumulation rate can be used, without adjustment, to estimate the ages of the older stratigraphic markers. The 720 cm-long piston core MAR02-113P in 298 m of water (39°24.184′N, 26°04.121′E; Fig. 2) and the seismic record at this site (Fig. 6) provide the basis for the following discussion. In this paper, conversions of acoustic two-way travel times to sub-seafloor depths are based on an acoustic velocity of 1500 m s^{-1} in water-saturated muds, so 10 ms (ms) two-way time (TWT) is equivalent to ~7.5 m sediment. Physical properties velocity data from the DSDP Site 378 from the southern Aegean Sea and the DSDP Site 380 from the Black Sea reveal that the unconsolidated P-wave velocities for the upper ~400 m range from 1471 m s^{-1} to 1600 m s^{-1} (Ericson, 1978; Shipboard Scientific Staff, 1978). Therefore, the 1500 m s^{-1} velocities used in this paper are representative of the true velocities for the unconsolidated sediments in the study area. Relevant calibrated radiocarbon dates and associated errors are presented in Table 1. Calibration was achieved using Oxcal 4.1 online software, the Marine09.14c calibration curve, and a reservoir age of 405 years.

Three approaches allow a reliable chronology to be developed. In the first approach, an age model was developed for core MAR02-113P. Five dated points in the core define a consistent sedimentation rate of 25 ± 1 cm/1000 years over the time interval ~11–30 ka (Fig. 7). Sedimentation rate during the Holocene (<11 ka) is in the range 16–20 cm/1000 years but is not well constrained because the amount of core-top loss during the piston-coring operation is uncertain (technical problems prevented retrieval of a gravity core at this site). The key reflector α occurs at a seismic depth of ~260 ± 50 cm (İşler et al., 2008), so its age is constrained by the age model to ~12–16 ka (Fig. 7).

The second approach involves radiometric dating of key reflector α_1 which occurs at a seismic depth of 38.2 ± 0.5 m below the MAR02-113P site (Fig. 6; İşler et al., 2008). Landward of the MAR02-113P site, reflector α_1 fortuitously occurs in one area at a depth sufficiently shallow that it was sampled in two closely

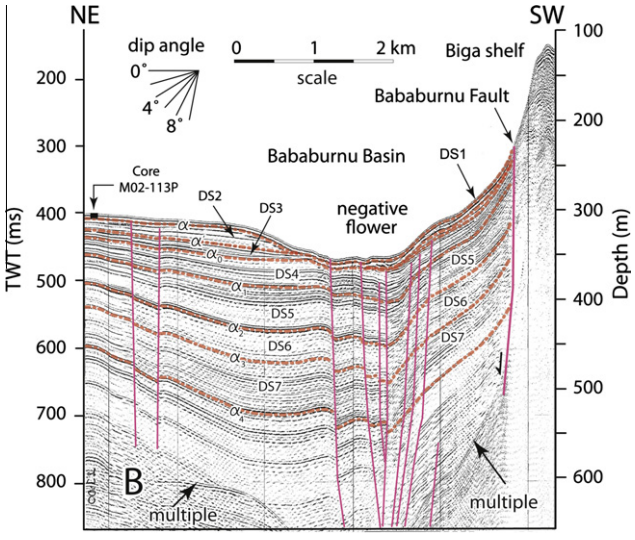

Fig. 6. Air-gun seismic reflection profile "**B**" across the eastern segment of the Bababurnu Basin showing the Bababurnu Fault and a series of smaller southwest- and northeast-dipping faults delineating a prominent graben. The soles of the faults converging at depth suggest that the graben is probably a negative flower structure. Also shown are the bounding unconformities α, α′, α_0, α_1, α_2, α_3, α_4, of depositional sequences (DS) 1 through 7 and the location and approximate depth of penetration of core MAR02-113P. See Fig. 2 for location.

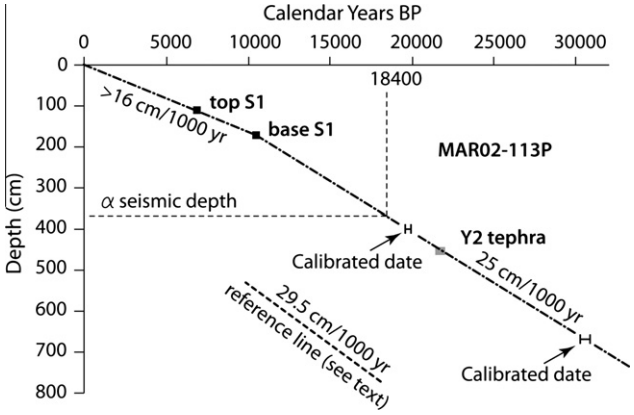

Fig. 7. Age model for core MAR02-113P based on data in Table 1. Symbol sizes indicate errors of one standard deviation in calibrated ages. Line segments are hand fitted to the plotted points. The 25 cm/(1000) year line cannot shift even a small amount without straying from data points. The 30 cm/(1000) year reference line reflects the average sedimentation rate determined by dating reflector α_1 (see text). The seismic depth of the α unconformity is from İşler et al. (2008).

Table 1
Table of radiometric ages. See Fig. 2 for localities. UQAM = U/Th dates from Université de Montréal. TO = ^{14}C dates from Isotrace Laboratories (University of Toronto; half-life of 5568 yr; errors represent 68.3% confidence limits). Calibration of raw ^{14}C dates from Oxcal 4.1 online software, the Marine09.14c calibration curve, and a reservoir age of 405 years. The Y2 tephra is mixed into surrounding muds by burrowers so its depth is picked as the midpoint of the tephra-bearing interval (MAR02-113P, 445–461 cm).

Core Number	Depth (cm)	Water depth (m)	Sample	Raw Age (C^{14} yr BP)	Laboratory code of source	Calendar age (cal yrBP)
MAR02-113	173	298	Base S1 sapropel	9600 ± 60	Aksu et al. (1995)	10450 ± 70
MAR02-113	400	298	Pecten spp.	16930 ± 140	TO-11151	19710 ± 190
MAR02-113	455	298	Y2 tephra		Eriksen et al. (1990)	21705 ± 311
MAR02-113	672	298	Serpulid worm tube.	26100 ± 250	TO-11152	30520 ± 275
MAR03-48	44	311	Ostrea sp		UQAM	118927 + 6193 − 5852
MAR03-49	270	321	Ostrea s		UQAM	133218 + 73118 − 6814

spaced piston cores MAR03-48P (39°28.351′N, 25°51.723′E) and MAR03-49P (39°28.102′N, 25°51.436′E, Fig. 2; İşler et al., 2008, their Fig. 18b). Two oyster shells were dated in these cores using U/Th methods (Table 1). One shell was ~100 cm above the inferred depth of α_1 and the other was only a few centimetres below the unconformity (İşler et al., 2008, their Fig. 16). Dating of molluscs by $^{230}Th/^{234}U$ methods is generally considered to be unreliable because U is considered to be labile in mollusc shells (Edwards et al., 2003). Therefore, the U/Th dates in oysters should be viewed with caution. However, the correlation between the sedimentary successions where these two U/Th ages are obtained and the seismic profiles showing that these oysters are extracted from the top of depositional sequence 5 (Işler et al., 2008) strongly suggest that the U/Th ages are reliable and that they representative of the true ages of these successions, Even with errors of one standard deviation, the two dates do not overlap. A conservative estimate of the age of α_1 includes the entire range between the two U/Th dates: 118.9–133.2 ka (Table 1). This is deemed to be conservative because the ~100 cm of sediment between the younger shell and the inferred unconformity represents perhaps 3000–4000 years of accumulation, and an unknown thickness of sediment above the older shell must have been removed by erosion along the unconformity. Combining maximum and minimum age estimates with the depth of α_1 at site MAR02-113P (38.2 ± 0.5 m) yields basinal sedimentation rates of 28.3–32.5 cm/1000 years. These rates are 13–30% higher than the estimate obtained using the age model for core MAR02-113P (Fig. 7), but are believed to better represent the long-term sedimentation rate because of the longer time interval used in this second calculation, encompassing an entire glacial–interglacial cycle (i.e. marine isotopic stages MIS5 to MIS1).

In addition to α and α_1, there are five other key seismic markers, α', α_0, α_2, α_3 and α_4, which occur respectively at sub-seafloor depths of 10.2, 17.7, 75.1, 101.9 and 126.4 m at site MAR02-113P (Fig. 6), based on an acoustic velocity of 1500 m s^{-1}. These five depths (with ±5 m errors) and minimum and maximum sedimentation rates of 28.3 and 32.5 cm/1000 years were used to calculate a realistic age range for each of the five key seismic markers (Table 2). The ages reported in Table 2 for α and α_1 are those determined earlier in this section.

The third approach uses sequence-stratigraphic arguments to more precisely define the ages of all seven key seismic markers. The key surfaces are unconformities in nearshore areas where they overlie seaward-prograded deposits interpreted by İşler et al. (2008) as deltas that advanced across the Aegean Sea shelf as sea level fell during Quaternary glacial cycles. Glacial–interglacial cyclicity and therefore Quaternary sea level mimics open-ocean oxygen-isotopic curves (e.g. Chappell and Shackleton, 1986) or insolation curves calculated on the basis of Milankovitch theory (Imbrie et al., 1984). Here, we use the global sealevel curve of Bintanja et al. (2005) (Fig. 8a) because the Aegean Sea was fully connected to the world ocean throughout the Quaternary. The radiometrically determined ages of unconformities α and α_1 coincide with the onset of global transgressions which developed at the terminations of glacial isotopic stages 6 and 2 (i.e. MIS 6 and MIS 2, Fig. 8b). Four of five indirectly dated markers (excluding α' – see İşler et al., 2008, for interpretation of this anomaly) also have age ranges which bracket times of significant global sea level rise (Fig. 8c). Helland-Hansen and Martinsen (1996) explain why basinal conformable surfaces traced seaward from lowstand unconformities on a shelf (i.e. the "sequence boundaries" of Mitchum et al., 1977) should coincide with the beginning of the next transgression. Hence, there are theoretical grounds for suggesting that the shelf-crossing unconformities (and correlative conformities) in the Aegean Sea correlate with the initial phases of what are mostly post-glacial transgressions. Using similar logic, Skene et al. (1998) concluded that deltas elsewhere in the Aegean Sea advanced basinward during glacial times and retreated during post-glacial transgressions, so that each depositional sequence correlates with a full glacial cycle, terminating with the development of a widespread key reflector/unconformity as the lowstand phase ended and sea level rise began. We use this theoretical underpinning to more tightly specify the ages of surfaces α' to α_4, and attach accuracies of ~±2 ka to these ages (Fig. 8d, Table 2). These estimates differ slightly from those of İşler et al. (2008) because of the incorporation of error bars in the present calculations and introduction of arguments based on basic principles of sequence stratigraphy. The age of the α unconformity is set to its maximum acceptable value in Table 2 in order to synchronize its development with the onset of the last post-glacial transgression. The ±2 -ka errors reflect uncertainty in placing our age picks on the transgressive legs of the sea-level curve of Bintanja et al. (2005). There is additional error because of age uncertainties in the sea-level curve itself; this is the case with all sea-level curves (Caputo, 2007) and will be taken into account in Section 7, Basin Subsidence.

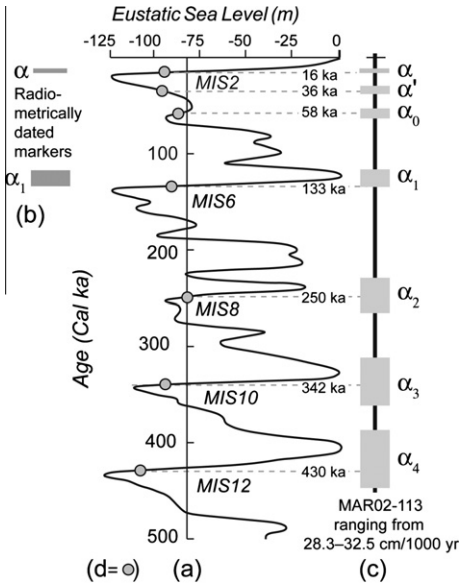

Fig. 8. (a) Global sea level curve from Bintanja et al. (2005) with labels for even-numbered marine isotopic stages (MIS), corresponding to times of continental glaciations. (b) Age ranges for seismic markers (shelf-crossing unconformities) α and α_1 determined using radiometric dates – these remain fixed in part c because they are constrained by hard data. (c) Permissible ranges of ages for seven seismic markers either transferred from part b or based on minimum and maximum sedimentation rates of 28.3 and 32.5 cm/(1000) years (Table 2). (d) Estimates of the ages of key seismic markers consistent with part c and following the arguments of Helland-Hansen and Martinsen (1996) that conformable equivalents of sequence boundaries should coincide with the onset of transgressions.

Table 2
Age estimates for seismic markers.

Name	Depth (m) beneath MAR02-113P	Permissible age range (ka)	Age based on concepts of sequence stratigraphy (ka)
α	2.10–3.10	12.0–16.0	16 + 0/−2
α'	9.7–10.7	29.8–37.8	36 ± 2
α_0	17.2–18.2	52.9–64.3	58 ± 2
α_1	37.7–38.7	118.9–133.2	133 ± 2
α_2	74.6–75.6	229.5–267.1	250 ± 2
α_3	101.4–102.4	312.0–361.8	342 ± 2
α_4	125.9–126.9	387.4–448.4	430 ± 2

6. Structural framework of the Bababurnu Basin and Biga Shelf

6.1. Basins and ridges delineated by acoustic basement

Seismic reflection profiles show that the shelf region north and northeast of the Bababurnu Basin includes three NE–SW-trending sedimentary basins (B1, B2 and B3) and two intervening ridges (R1 and R2 in Figs. 9 and 10; also see İşler et al., 2008). In seismic reflection profiles, the ridges appear as narrow anticlines cored by elevated pre-Quaternary acoustic basement (Fig. 9). The intervening basins delineate open synclines variably filled with Quaternary sediments, which are thickest along the basin axes and show dramatic thinning toward the ridges. This convergence occurs as progressive west- and east-directed onlap associated with variable amounts of erosion beneath shelf-crossing unconformities (Fig. 9). In the southern and southwestern portions of the study area, the ridges are only blanketed by a thin veneer of sediments (20–25 ms thick); however, toward the north, they are largely exposed at the seafloor. These small shelf basins and their intervening ridges plunge toward the south and southwest. While basin B2 is entirely confined to the Biga Shelf, basins B1 and B3 merge in deeper water depths with the Bababurnu Basin and the North Skyros Basin, respectively (Fig. 10; İşler et al., 2008).

6.2. Quaternary architecture

The Quaternary architecture of the northeastern Aegean Sea between the Islands of Bozcaada, Lesvos and Limnos is characterized by a series of broadly NE–SW- and E–W-striking faults (Fig. 10). On the basis of temporal and spatial distribution of faults, the position of the tip points, and the amounts of displacement of the stratigraphic successions across the fault planes, two domains are identified in the study area: (i) a basinal domain (herein referred to as the Bababurnu Basin), and (ii) a shelf domain (herein referred to as the Biga Shelf).

6.3. Bababurnu Basin

A shaded bathymetric map constructed using soundings collected during the cruises in 1998, 2000, 2002 and 2003, demonstrates the presence of a 300 m-deep rhombohedral basin in the study area (i.e., the Bababurnu Basin; Figs. 3 and 10). The structure in this domain is characterized by several WNW- and SE-striking planar faults which have near straight and rarely curvilinear map traces. These faults display moderate to high northerly or southerly dips, ranging from 40° to 60°. A dense grid of seismic reflection profiles (Fig. 2) provides the basis for fault correlations between adjacent seismic profiles, thus allowing a detailed fault map to be constructed (Fig. 10).

One of the prominent faults of this group is the Bababurnu Fault, an arcuate, SW-convex, predominantly SE-striking (~115°) and SW-dipping faults which normal-sense dip separations (Figs. 6, 11 and 12). Traced toward the east, the fault progressively swings toward the east/northeast, and runs nearly parallel to the southern shores of the Biga Peninsula (Fig. 10). Traced westward, the Bababurnu Fault abuts a prominent NE-striking fault, herein referred to as the Biga Fault (Fig. 10). The Bababurnu Fault gives the appearance of a through-going master fault as it transects Bababurnu Basin with a relatively straight map trace. A series of short seismic reflection profiles show the spatially consistent appearance of this through-going master fault (Figs. 6, 11 and 12). The tip point of the fault often extends to the depositional surface where it creates a remarkable scarp on the seafloor, with vertical separations of the seabed ranging between 45 m and 200 m (Figs. 6, 11 and 12). A comparison between the bathymetric and structural maps reveals that the Bababurnu Fault delimits the fault-controlled shelf-slope break in the southeastern portion of the study area (Fig. 10). The sedimentary successions in the footwall and hanging wall of the fault exhibit notable differences. For example, the upper section of depositional sequence 4, composed of oblique-prograded clinoforms, is absent in the hanging wall of the Bababurnu Fault (Fig. 13). Assuming that the rate of sediment input to the basin was constant, the absence of oblique-prograded clinoforms suggests that during the time of development of depositional sequence 4, noticeably higher rates of subsidence prevailed on the hanging wall block of the Bababurnu Fault which, in turn, created water depths too deep for delta progradation.

Biga Fault is another major, broadly NE- and ENE-striking (45–80°), SE-dipping fault with a normal-sense dip slip (Figs. 5, 10 and 13). Similar to the Bababurnu Fault, the Biga Fault also behaves as a basin-bounding fault, delimiting the northwestern boundary of Bababurnu Basin (Fig. 10). It creates a prominent bathymetric step on the seafloor with vertical seabed separations ranging between 15 m and 127 m (Figs. 5 and 13). Correlation of marker reflectors across the fault shows that the depositional sequences are invariably thicker in the hanging wall, where they form prominent sedimentary wedges that thicken toward the fault plane. Traced to the northeast, the vertical seabed offsets of Biga Fault progressively diminish to ~4 m, and the fault loses its bathymetric expression, becoming indistinguishable from any of the minor faults mapped in this area (Figs. 3 and 10). Along the central portion of the Biga Fault, the sedimentary successions are locally folded in the vicinity of the fault, perhaps because of drag along the fault plane (Figs. 5 and 13). The folded geometry extends parallel to the fault and can be traced for more than 10 km along the fault. In the south-

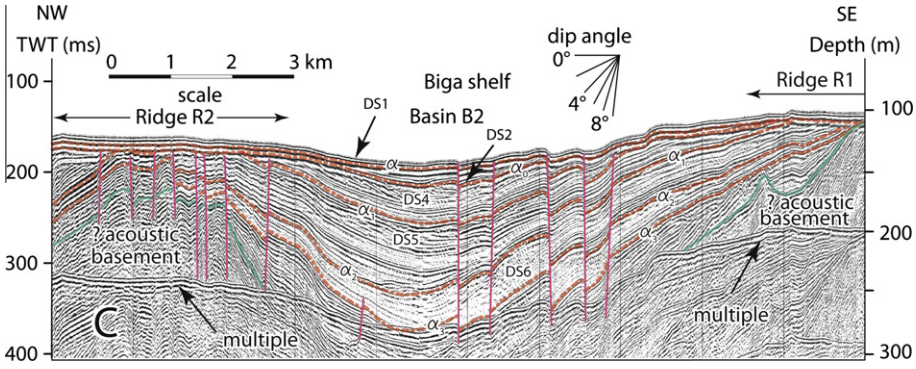

Fig. 9. Air-gun seismic reflection profile "**C**" across the southwestern Biga Shelf showing the internal architecture of ridges R1 and R2 and the intervening basin B2. Note that depositional sequences (DS) 6 and 4 dramatically thin toward the crests of the ridges, and that depositional sequence 4 is largely truncated by the shelf-crossing unconformity α. Also note that the ridges appear to be cored by acoustic basement.

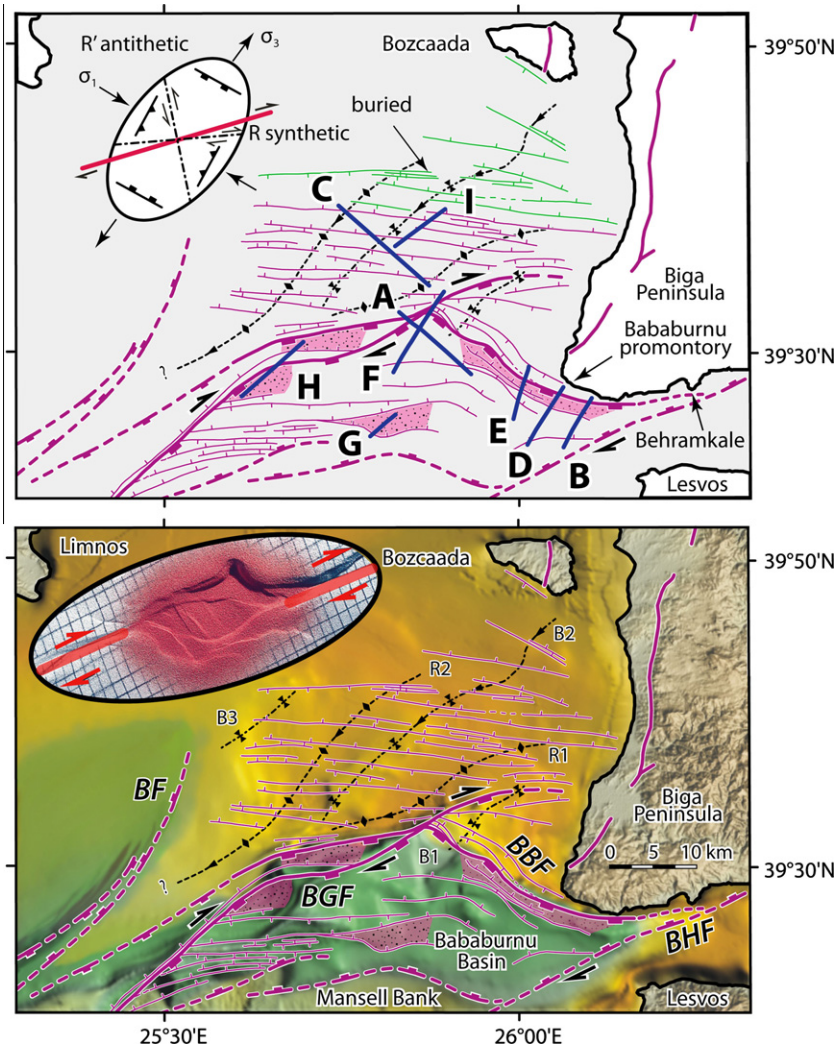

Fig. 10. (Top): Detailed tectonic map of the study area showing normal faults (ticks on hanging wall). Continuous and dashed lines represent mapped and speculated faults, respectively. Half arrows depict suggested strike-slip movements on faults. Thick blue lines with letters A through I are seismic profiles illustrated in figures. Dotted hachure with pink shade denotes zones characterized by en échelon faults. Thin black dashed lines with filled diamonds and bow-ties mark the crests of anticlines and synclines, respectively, while arrow-heads on dashed lines show the plunge direction of the anticlinal and synclinal hinge lines. Also shown is the strain ellipsoid for a dextral strike-slip fault (red line), the positions of the σ_1 and σ_3 axes of stress, as well as the R and R' orientations. A seismic line published by Saatçılar et al. (1999) shows the presence of a major horst along the strike of ridge R2 bounded by two prominent normal faults suggesting that the Bozcaada Fault extends nearly parallel to the Biga Fault both labeled in the bottom part of the figure as BF and GBF, respectively. (Bottom) Detailed tectonic map of the study area superimposed on the shaded bathymetry map, showing the strong correspondence between the bathymetry and tectonic elements. BBF: Bababurnu Fault, BGF: Biga Fault, BF: Bozcaada Fault, BHF: Behramkale Fault. R1 and R2 are ridges cored by acoustic basement, whereas B1 (trending into the Bababurnu Basin), B2 and B3 (trending into the North Skyros Basin) are Quaternary-Recent basins. Also shown is the analogue model for a 150° releasing sidestep pull-apart basin from Dooley and McClay (1997). (For interpretation of the references to color in this figure legend, the reader is referred to the web version of this article.)

west, the fold has a half-wavelength of ~1.5 km and amplitude of ~150 ms (~112 m). Toward the northeast, these dimensions progressively diminish to a half-wavelength of ~1 km and amplitude of ~100 ms (~75 m).

6.4. En échelon faults

A number of narrowly-spaced clusters of en échelon faults are recognized within the western part of the Bababurnu Basin (Figs. 10, 14 and 15). Each cluster is composed of several vertical to sub-vertical, NE- and SW-dipping, NW-striking faults that display normal- and reverse-sense dip–slip separations. The tip points of the faults lie near or at the seabed: emergent faults create 2–20 m steps on the seafloor, whereas buried faults create minor flexures and undulations on the seabed (Fig. 15). Detailed examination of the footwall and hanging wall cutoffs of marker reflectors shows that the vertical separations across these faults progressively increase down section. The internal architecture of the sedimentary strata within the hanging wall and footwall zones differs remarkably, ranging from relatively undisturbed, to moderately to highly folded and tilted. The fault bundle can be traced to adjacent seismic profiles; however, individual faults cannot be traced with certainty across the fault zone.

Within the deeper portions of the Bababurnu Basin, near the prominent Bababurnu Fault, a distinct narrow zone is recognized, consisting of 5–15 NE- and SW-dipping, sub-vertical and concave-upwards faults with normal sense dip–slip separations (Fig. 6). The zone is ~20 km long and ~3 km wide and runs parallel to the map trace of the Bababurnu Fault (Figs. 6 and 10). Along the zone, the faults display radical changes on adjacent seismic profiles in terms of spacing, number, sense of slip and fault-plane angle. The tip points of the faults lie near or at the seabed, creating 5–

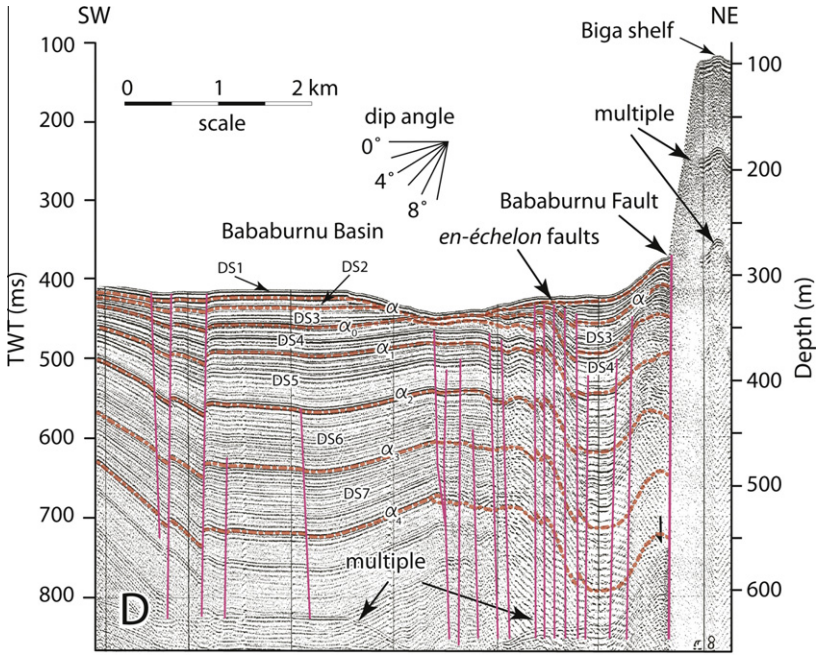

Fig. 11. Air-gun seismic reflection profile "**D**" across the eastern segment of the Bababurnu Basin showing the Bababurnu Fault and a series of smaller southwest- and northeast-dipping faults delineating a prominent graben. Note that the small faults along the southwest portion of the graben form en échelon sets. Also shown are the bounding unconformities α, α′, α_0, α_1, α_2, α_3, α_4, of depositional sequences (DS) 1 through 7. See Fig. 2 for location.

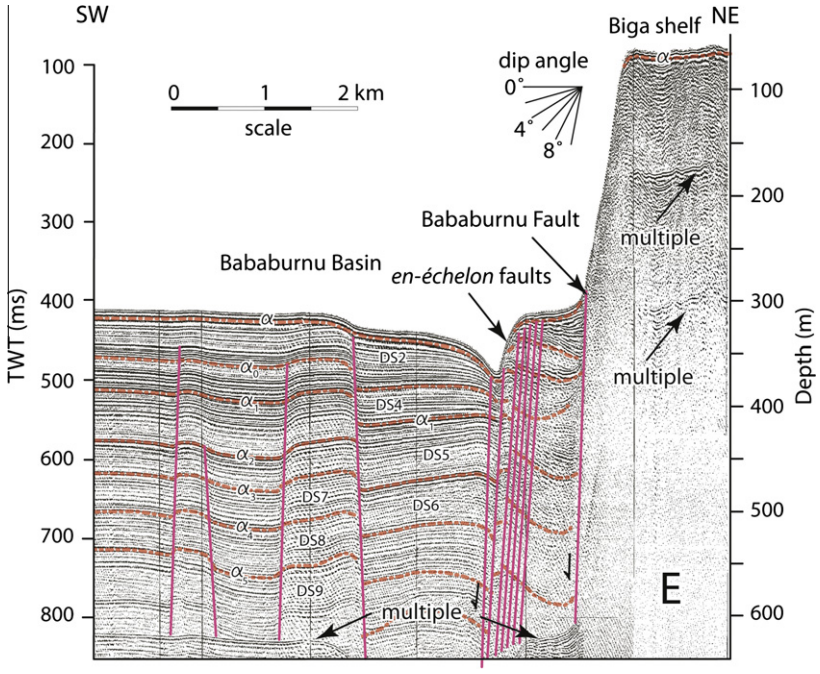

Fig. 12. Air-gun seismic reflection profile "**E**" across the central segment of the Bababurnu Basin showing the Bababurnu Fault and small southwest- and northeast-dipping faults delineating a graben. Also shown are the bounding unconformities α, α′, α_0, α_1, α_2, α_3, α_4, α_5 of depositional sequences (DS) 1 through 9. Note that the Bababurnu Fault creates ~250 m displacement across the fault. See Fig. 2 for location.

55 m steps on the seafloor. With increasing depth below the seabed, the dip angles of the faults gradually steepen and several faults appear to converge, giving the impression that they probably eventually merge to create a single stem below the imaging depth of the seismic profiles. As a whole, this architecture is interpreted as a negative flower structure. These very narrowly spaced faults result in the chaotic seismic configuration of the reflections. These faults locally change their dip direction and display larger vertical separations.

Many aspects of the cross-sectional structural patterns identified within the study area are characteristic of strike-slip deformation. These include: (1) a steeply dipping solitary master fault that displaces all the observed sedimentary cover and exhibits a through-going, curvilinear map trace (Bababurnu Fault and Biga

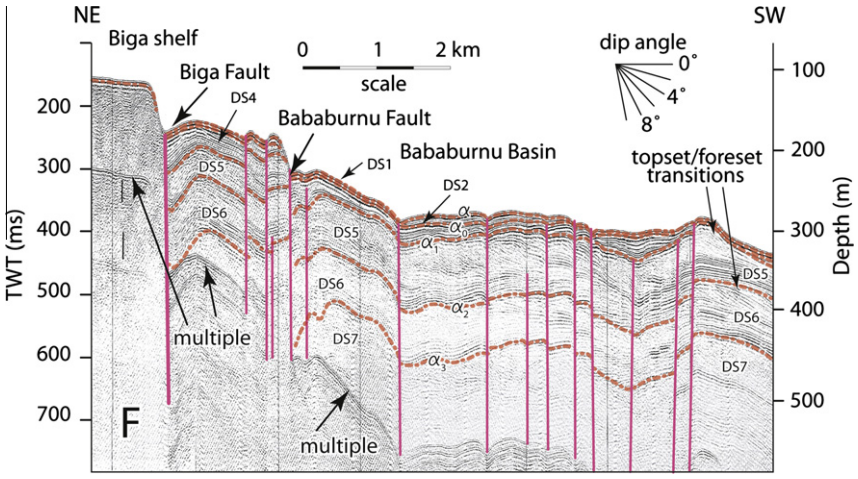

Fig. 13. Air-gun seismic reflection profile "**F**" across the western segment of the Bababurnu Basin showing the Bababurnu and the Biga Faults and small southwest- and northeast-dipping faults delineating a graben. Also shown are the bounding unconformities α, α', α_0, α_1, α_2, α_3 of depositional sequences (DS) 1 through 7. See Fig. 2 for location.

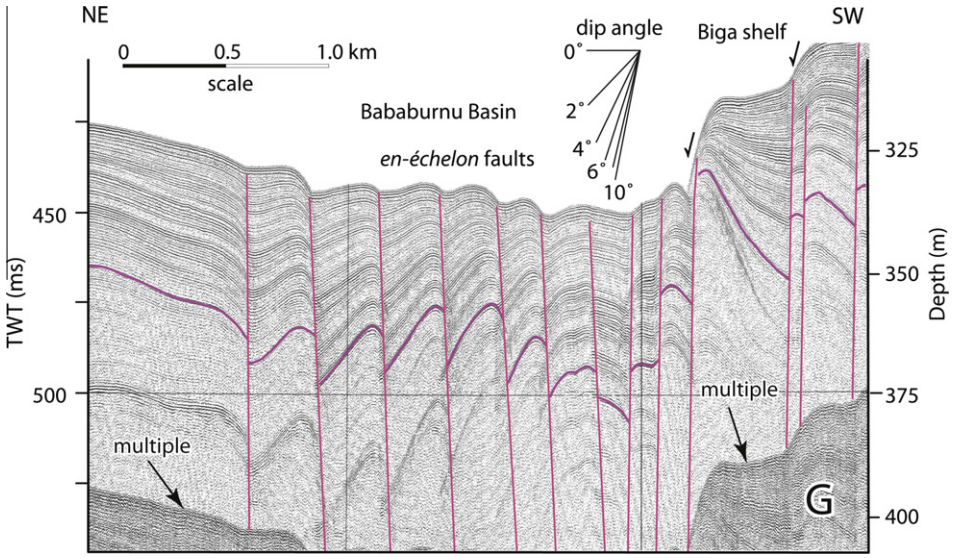

Fig. 14. Huntec deep tow system seismic reflection profile "**G**" across the south-central Bababurnu Basin south of Mansell Bank showing the series of prominent en-échelon faults. An upper Quaternary marker is highlighted to show the fault separations. See Fig. 2 for location.

Fault (e.g., Figs. 5, 6, 10, 11 and 13); (2) upward splaying sub-vertical faults defining negative flower structures (e.g., Fig. 6); (3) zones of intense deformation isolated between comparatively undeformed areas (e.g., Fig. 15); (4) simultaneous development of both extensional and contractional structures in individual transverse profiles within the same local area (e.g., Fig. 15); (5) en échelon arrangement of the faults (e.g., Figs. 10, 14 and 15); (6) along-strike changes in the dip direction of a right-lateral shear zone (e.g., Figs. 5 and 6); and (7) juxtaposed sedimentary thickness contrasts of the same depositional sequences in the footwalls and hanging walls of the faults (e.g., Figs. 5, 6 and 13).

En échelon faults observed in the study area are interpreted to form as a consequence of strike-slip deformation. Faults occurring immediately south of the through-going Bababurnu Fault appear to be antithetic normal to oblique faults that define a negative flower structure (e.g., Fig. 6). These faults must have developed during the evolution of the Bababurnu pull-apart basin. The en échelon faults along the northwestern and southeastern segments of the Biga Fault as well as the southern margin of the Mansell Bank (Fig. 10) are interpreted as splays of these through-going faults, as they trend oblique to these major faults, merging with them along strike.

6.5. Biga Shelf

The structural architecture of the Biga Shelf is characterized by several WNW-striking, ENE- and WSW-dipping planar faults (Fig. 10). In seismic reflection profiles, the faults display moderate- to high-angle dips ranging between 50° and 60° (Fig. 16). These faults obliquely transect the broadly NE-trending basins and ridges delineated by the acoustic basement (Fig. 10). Detailed examination along the fault planes shows that the footwall and hanging wall cutoffs of marker reflectors and shelf-crossing unconformities show normal sense vertical stratigraphic separations, with separations range from <1 m to ~10 m. The footwall and hanging wall cutoffs of marker reflectors, such as the shelf-crossing unconformities, show mild to moderate growth within the hanging walls (e.g., Fig. 16), suggesting that the faulting is syn-sedimentary. Most

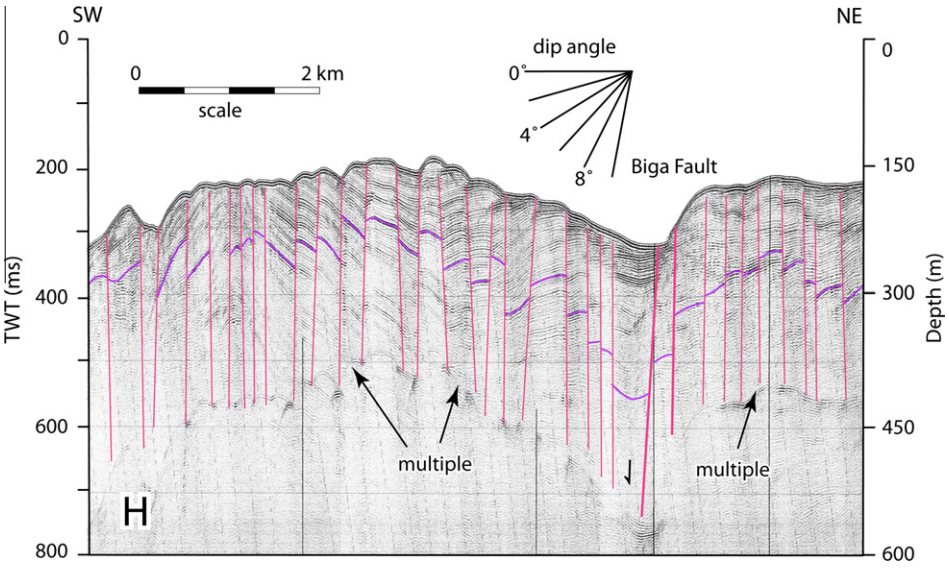

Fig. 15. Sparker seismic reflection profile "**H**" across the western Bababurnu Basin, immediately southeast of the Biga Fault showing the very prominent en-échelon faults. An upper Quaternary marker is highlighted to show the fault separations. See Fig. 2 for location.

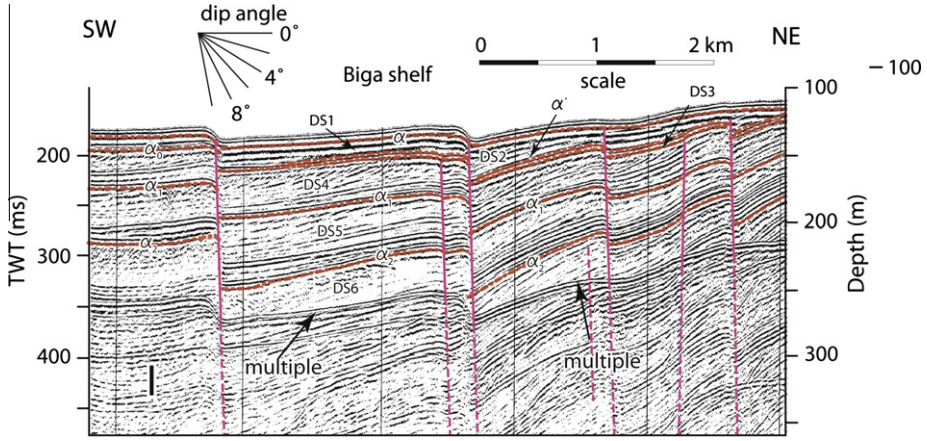

Fig. 16. Airgun seismic reflection profile "**I**" across the Biga Shelf showing various faults cutting the stacked prograded delta successions. Note the mild to moderate sedimentary growth on the hanging walls of faults. Also shown are the bounding unconformities α, α', α_0, α_1, α_2 of depositional sequences (DS) 1 through 6. See Fig. 2 for location.

faults in the southern segment of the Biga Shelf have tip points at the seafloor or lying immediately below the α unconformity, and create distinct steps on the seafloor. On the other hand, most (if not all) faults in the northern segment of the Biga Shelf are buried and have tip points that lie well within the Quaternary successions and create no inflection on the seafloor (Fig. 10a).

7. Basin Subsidence

Glacio-eustatic sea-level fluctuations, relative sea-level variations caused by tectonic movements (emergence and subsidence), and style of sedimentation are the principal factors that controlled the Quaternary-Recent stratigraphic architecture observed in the study area. The seaward-prograded successions are interpreted as delta lobes (İşler et al., 2008; their Fig. 12). Their vertical stacking requires significant tectonic subsidence to account for the long-term creation of accommodation space. If there had been no subsidence, each depositional sequence that developed during a phase of sea-level lowering and the subsequent lowest stand of sea-level would have accumulated in front of the previously deposited depositional sequence, resulting in a seaward-prograded shelf break.

The amount of tectonic subsidence can be calculated by measuring the difference in vertical elevation between (a) the topset-to-foreset transition of an ancient depositional sequence of known age and (b) the elevation of the same break-in-slope in similar modern deltas. The only other parameter that must be known is the height of sea level at the time delta progradation stopped (relative to the modern sea-level datum). The age of the most seaward topset-to-foreset transition of Quaternary Aegean Sea deltas proceeds by only a few thousand years the age of the immediately overlying key reflector because key surfaces (unconformities and their correlative conformities) correlate with the initial stages of flooding of former lowstand deltas (cf. Helland-Hansen and Martinsen, 1996). Uncertainties in the ages of both the key reflectors and the topset-to-foreset transitions include an estimated ±2 ka plotting error (Fig. 8d) and a somewhat larger uncertainty that exists for the sea-level curve used in the analysis. Caputo (2007) reports age uncertainties for a number of sea-level curves of ±5 ka for ages <110 ka and potentially as much as ±15 ka for ages in the

range 110–420 ka. Caputo (2007) also recommends using an uncertainty of at least ~15 m in ancient water levels derived from a range of Quaternary sea-level curves. The topset–foreset transitions of modern Aegean Sea and Mediterranean Sea deltas occur at water depths of ~15–20 m (Aksu and Piper, 1983; Aksu et al., 1987, 1992a, 1992b). Please note that if the velocity estimates of 1500 m s^{-1} is underestimated by ~10%, the subsidence rate would also be underextimated by ~10%.

Clearly, the interpretation of the elevation of the topset-to-foreset transition of an ancient delta must take into account both the probable paleo-water depth (~20 m) and the sea level in the basin at the time of deposition. For example, if the ancient sea level was 100 m lower than today, then a topset-to-foreset transition found today at an elevation of −120 m would require no post-depositional subsidence, just inundation by rising water levels (for simplicity, this example neglects isostatic loading by seawater).

In the following calculations, we incorporate the following uncertainties: ±7 ka in the ages of topset–foreset transitions younger than 110 ka; ±17 ka in the ages of topset–foreset transitions older than 110 ka; ±15 m in ancient sea levels picked from the curve of Bintanja et al. (2005); ±5 m in elevations picked from seismic profiles. Water depth over topset-to-foreset transitions is set at 20 m. No allowance is made for the water load that currently lies above the buried deltas. Because we do not have sufficient knowledge of the flexural rigidity in the area, which would control the amount of subsidence generated by variations of water load across the shelf and into the deeper basin. Certainly a consideration of this water load would slightly reduce the calculated amount of subsidence and subsidence rates. However, relative differences in subsidence rates between shelf and basinal areas would remain correct. In basins B1 and B2, most of the topset-to-foreset transitions below depositional sequences 2 and 3 cannot be imaged due to the limited seismic coverage and the presence of seafloor multiples that mask the lower portions of the seismic profiles. In Bababurnu Basin, the topset-to-foreset transitions in depositional sequences 4–7 are imaged (e.g., Fig. 5), while in basin B1 only the transition for depositional sequence 7 is observed.

The topset-to-foreset transition for depositional sequence 4 is best imaged in the Bababurnu Basin (e.g., Figs. 5 and 13). It occurs ~168 ms (−126 ± 5 m) below present sea level. Depositional sequence 4 developed during interglacial isotopic stage 5 (for Subunit 4b, Işler et al., 2008) and the subsequent glacial isotopic stage 4 (for Subunit 4a; İşler et al., 2008), terminating at 62 ± 7 ka when sea level stood at −92 ± 15 m. If the topset-to-foreset transition was 20 m below the paleo-sea level, then it must have subsided from −92 − 20 m = −112 ± 15 m to its current −126 ± 5 m, corresponding to a net subsidence of 14 ± 20 m (so possibly slight uplift). The subsidence rate needed to accomplish this drop in elevation over the available time interval is 23 ± 33 cm kyr^{-1} (Table 3). In this case, uncertainties in the input parameters allow the possibility of slight uplift, but the overall stacking of deltaic cycles throughout the study area makes it more reasonable to conclude that subsidence also occurred at this site, but at a very slow rate.

The topset-to-foreset transition in depositional sequence 5 occurs at elevations of ~230 ms (−173 ± 5 m) on the shelf, while in structurally deeper parts of the Bababurnu Basin it occurs at depths ranging between ~371 ms (−278 ± 5 m) and ~410 ms (−308 ± 5 m) below present sea level (e.g., Figs. 5 and 9). Depositional sequence 5 developed during interglacial isotopic stage 7 (for Subunit 5b) and the subsequent glacial stage 6 (for Subunit 5a; Işler et al., 2008), terminating at 138 ± 17 ka when sea level stood at −125 ± 15 m. This paleo-sea level and a 20 m paleo-water depth imply that, since the initiation of interglacial oxygen isotopic stage 5, Bababurnu Basin experienced subsidence ranging between 133 ± 20 m and 163 ± 20 m, whereas the adjacent shelf saw less subsidence: 28 ± 20 m. These values suggest basinal subsidence rates of 98 ± 19 and 120 ± 21 cm kyr^{-1}, respectively, and rates closer to basin margins of 21 ± 15 cm kyr^{-1} (Table 3).

Table 3
Subsidence rates calculated using the topset-to-foreset transitions in prograded delta successions, the sea-level curve of Bintanja et al. (2005), and assuming a paleo-water depth of 20 m over topset-to-foreset transitions. Errors in subsidence rates are one standard deviation about the mean calculated using five combinations of elevation differences and ages; each evaluated with a different set of maximum and minimum input parameters based on ± uncertainties explained in the text.

Depositional sequence	Depth topset–foreset transition (m)	Depth of global sea-level (m)	Subsidence rate (cm kyr^{-1})
DS4	126 ± 5	−92 ± 15	23 ± 33
DS5	−173 ± 5	−125 ± 15	21 ± 15
	−278 ± 5	−125 ± 15	98 ± 19
	−308 ± 5	−125 ± 15	120 ± 21
DS6	−360 ± 5	−92 ± 15	99 ± 10
DS7	−430 ± 5	−112 ± 15	87 ± 7
	−261 ± 5	−112 ± 15	39 ± 5

Depositional sequence 6 developed during the interglacial and glacial stages 9 and 8, respectively, and spans a time interval of ~92,000 yr. The youngest topset-to-foreset transition developed at about 252 ± 17 ka (Figs. 8a and 13). The transition is imaged in the southeast portion of Bababurnu Basin and lies ~480 ms (−360 ± 5 m) below present sea level. During the last phase of progradation, sea level stood at −92 ± 15 m. The present depth of the topset-to-foreset transition and the paleo-sea-level position suggest that the area has subsided 248 ± 20 m since 252 ± 17 ka at a subsidence rate of 99 ± 10 cm kyr^{-1} (Table 3).

Depositional sequence 7 formed during global isotopic stages 11 and 10 (between the time of formation of reflectors α_4 and α_3, (Fig. 8a). Seismic reflection profiles show that the topset-to-foreset transition in depositional sequence 7 occurs at ~574 ms (−430 ± 5 m) in Bababurnu Basin and at ~348 ms (−261 ± 5 m) in basin B2 (e.g., Figs. 5 and 9). The final phase of delta progradation ceased at ~345 ± 17 ka. At that time the sea level stood at −112 ± 15 m. These data indicate subsidence amounts of 298 ± 20 m and 129 ± 20 m for Bababurnu Basin and basin B2, respectively, which correspond to subsidence rates of 87 ± 7 cm kyr^{-1} in Bababurnu Basin and 39 ± 5 cm kyr^{-1} in basin B2 (Table 3).

The magnitude of global sea-level variations, and the rates of tectonic subsidence (or emergence) and sediment input control the thickness of a depositional sequence. If each sea-level fall was of similar magnitude and the rate of tectonic subsidence and sediment input were constant, then the depositional sequences that would develop during consecutive glacial–interglacial cycles would have the same thicknesses throughout the study area, provided that the durations of the successive interglacial and glacial isotopic stages were the same. For example, the upper section of depositional sequence 4 is composed of oblique-prograded clinoforms: this section is absent in the hanging wall of the Bababurnu Fault (Fig. 8A). Assuming that the rate of sediment input to the basin was constant, the absence of oblique-prograded clinoforms suggests that noticeably higher rates of subsidence prevailed on the hanging wall block of the Bababurnu Fault during the time of development of depositional sequence 4, which in turn, created water depths too deep for delta progradation. Seismic reflection profiles show that depositional sequences exhibit significant thickness variations in different basins across the study area. For instance, in the Bababurnu Basin the thicknesses of the depositional sequences are nearly twice those observed in basins B1 and B2 (e.g., compare Figs. 5, 6, 9, 11 and 13; also see İşler et al., 2008, isopach maps in their Fig. 12). The dramatic thickness variations might be the result of different subsidence rates. For

example, the difference in the thickness of depositional sequence 5 in basins B1 and B2 is ~30 ms (~23 ± 5 m). During the development of depositional sequence 5, the rate of creation of accommodation space in basin B2 must have been slower than that in basin B1, leading to a greater amount of sediment bypass across the shelf area and lesser amounts of sediment accumulation in basin B2. Bypassed sediments are advected offshore by waves and longshore currents and would most likely have been deposited within the deeper portions of the study area where low-energy conditions prevailed.

Subsidence rate on what is now the shelf and along basin margins has been no more than 20–35 cm kyr^{-1} while deeper portions of Bababurnu Basin experienced much higher rates from potentially 80–140 cm kyr^{-1} when uncertainties are considered (Table 3). The values for the shelf region are in good agreement with previously published values for the central, northern and northwestern Aegean Sea (e.g., (Piper and Perissoratis, 1991; Lykousis, 2009).

8. Discussion

8.1. Western extension of the middle strand of the North Anatolian Fault

The most prominent structural elements observed in the study area include major normal faults, the NE–SW-trending ridges R1 and R2 and their intervening basins B1 (and its deeper water extension, the Bababurnu Basin), B2 and B3 (and its deeper water extension, the North Skyros Basin). The Bababurnu and Biga Faults constrain the temporal and spatial distributions of all other faults in the study area (Figs. 1B and 10). The ridges and probably the basins constitute the basement in the study area, although the pre-Quaternary elements of the basins are not observed in the seismic reflection data. The origin of the basement rocks cannot be unequivocally determined due to the lack of well data and limited acoustic penetration of the existing seismic reflection profiles. Yaltırak and co-workers (Yaltırak et al., 1998, 2000a) interpreted the folded acoustic basement as mainly Miocene successions, and proposed that the folding occurred during the development of thrusting on the Gelibolu Peninsula (Kreemer and Chamotrooke, 2004). Limited deeper penetrating seismic reflection profiles suggest that the Lower Miocene to Quaternary sequences are >1 km thick within the Bababurnu Basin (Boztepe-Güney et al., 2001).

The overall NE–SW-trending (~N35°E) ridge R1 on the Biga Shelf can be tentatively correlated with the similar-trending (~N40°E) Biga Mountains on the adjacent landmass (Fig. 4). This general trend in fold axes is very similar to those observed across northwestern Anatolia, including the Biga and Gelibolu Peninsulas and the region that extends between the Islands of Gökçeada, Bozcaada and the Strait of Çanakkale (Dardanelles), suggesting a regional fabric with a common compressional origin (Yaltırak et al., 2000a; Yaltırak, 2002).

Taymaz et al. (Sakınç and Yaltırak, 2005) pointed out that the northeastern portion of the North Skyros Basin is connected to the straight northern coast of Edremit Bay by narrow ENE-striking deep basins. This study clearly shows that there is no connection between the North Skyros Basin and Edremit Bay. In contrast, ridge R2 between the Bababurnu Basin and the North Skyros Basin (Fig. 10) displays morphological characteristics which are similar to the Western Saros Ridge between the North Aegean Through and Saros Basin (Papanikolaou et al., 2002). Ridge R2 is delimited by the Bozcaada and Biga Faults, two right-lateral oblique-slip faults with opposite dip–slip components (Figs. 1B, 10 and 17). The trend of ridge R2 perfectly matches the N30°E strike of the Biga Fault (Fig. 10). Therefore, the oblique-slip character of the Biga

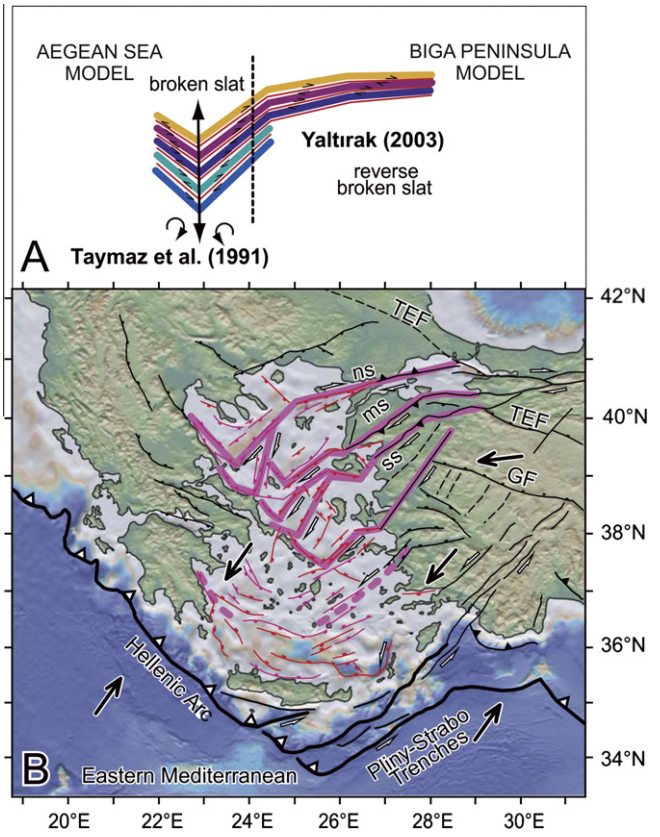

Fig. 17. Tectonic model explaining the evolution of the NE Aegean Sea. A: Map view of the broken slat (Taymaz et al., 1991) and asymmetric broken slat model in the Biga Peninsula (Yaltırak, 2003). B: Simplified tectonic map of the Aegean region for model correlation. Faults compiled from IGME (1989), Mascle and Martin (1990), Yaltırak et al. (1998), Papanikolaou et al. (2002), Yaltırak (2002, 2003) and Aksu et al. (2009). Topography and bathymetry are from Digital Elevation Model using GeoMapApp data base (Ryan et al., 2009).

Fault can be inferred to apply along the entire lineament. Mascle and Martin (1990) interpreted North Skyros trough as a NE–SW-trending asymmetric graben bounded along its southern side by important normal faults showing strike-slip deformation of the sedimentary cover in the North Skyros Basin. The NW-dipping, NE–SW-striking major fault imaged on the south side of this graben by Mascle and Martin (1990) matches perfectly the trend of the Bozcaada Fault (Fig. 10). We interpret the Bozcaada Fault as a major fault strike-slip fault which also shows normal-sense separation in the seismic reflection profiles.

Boztepe-Güney et al. (2001) also recognized the same zone designated as the Bababurnu Fault in this study. They interpreted the fault as one of a number of synthetic normal faults related to major faults seen onshore. The Bababurnu Fault continues farther east beyond the study area, but lack of seismic data precludes the eastward tracking and correlation of this fault with faults on land. However, the E–W- and NW–SE-striking map trace, significant displacement amounts along the fault, the existence of strike-slip deformation proximal to the fault, and its linkage with the SW-trending Biga Fault strongly suggest that the Bababurnu Fault defines the seaward extension of the middle strands of the North Anatolian Fault Zone (see below).

The number of strands of the North Anatolian Fault Zone trending into the Biga Peninsula and the positions of these strands are hotly contested. There are two major views: two-strand model with northern and southern strands (Siyako et al., 1989; Boztepe-Güney et al., 2001; Yılmaz and Karacık, 2001) and a three-strand

model with northern, middle and southern strands (Barka and Kadinsky-Cade, 1988; Yaltırak, 2002).

There is no disagreement with regards to the geographic position of the northern strand of the North Anatolian Fault Zone: all authors agree that it runs along the Marmara Sea and exits into the Aegean Sea across Saros Bay. Yılmaz and Karacık (2001) suggested a two-strand model, where the southern strand skirts the Uluabat and Manyas Lakes, deviates toward the SW at the town of Gönen, continues on the same trend and reaches Edremit Bay near Altınoluk (Fig. 4). The fault then deflects toward the west, and delimits the northern coast of Edremit Bay. These authors reported vertical displacements of as much as 500 m along Edremit Bay. They further pointed out a sinistral strike-slip component for this fault and interpreted it to be the northern bounding fault of the Edremit Graben. In contrast, Yaltırak (2002, 2003) proposed a three-strand model for the western extension of the North Anatolian Fault Zone where the middle strand follows the southern coastline of the Marmara Sea near Gemlik, deviating southward into Bandırma Bay, continuing in a NE–SW direction and exiting into Edremit Bay near the town of Behramkale. This strand is placed further west than the southern strand proposed by Yılmaz and Karacık (2001). In this paper, we suggest that the middle strand of the North Anatolian Fault Zone follows the route suggested by Yaltırak (2002, 2003), then deviates toward the west off Behramkale and continues farther westward as the Bababurnu Fault (Figs. 1 and 10). According to this proposal, the overall trend of the middle strand of the North Anatolian Fault Zone, starting from Behramkale and extending as far as the Bababurnu Basin, creates an ~E–W- then a NE–SW-trending, through-going map trace. The fault changes its direction west of the Bababurnu promontory to form a releasing bend along this dextral-slip fault (Fig. 10). This particular region would therefore be expected to consist of a rhomboidal pull-apart basin. However, this geometry is not clear for the Bababurnu Basin because of a lack of seismic data at its southern boundary.

The geometry of Bababurnu Basin has remarkable similarities to features in the analogue model constructed by Dooley and McClay (1997). During the initial stages of the analogue experiment, step-over faults developed at the top of the modeled basement as a result of shear forces (Dooley and McClay, 1997; their Figs. 2 and 7). We scaled displacements measured in the analogue model to the dimensions of features in the Bababurnu Basin (Fig. 10). A 5–10 cm model displacement is comparable to 7–14 km of right-lateral movement on the Bababurnu step-over faults. Other researchers working on the middle strand of the North Anatolian Fault Zone have recorded 7–8 km displacement in Edincik (Siyako et al., 1989), Gemlik Bay and Iznik Lake (Yaltırak and Alpar, 2002a; Öztürk et al., 2009),

8.2. Tectonic evolution of the basins in the Aegean Sea

The literature regarding the Quaternary tectonic evolution of the Aegean region is in a state of flux, particularly the cause(s) of the extensional tectonics and the development of a series of broadly E–W-trending graben. Three models have been proposed: (1) back-arc extension associated with the southward roll back of the Hellenic Arc (Biju-Duval et al., 1977; Hsü et al., 1977; Le Pichon and Angelier, 1979, 1981; McKenzie and Yılmaz, 1991; Bozkurt and Oberhansli, 2001; Pe-Piper and Piper, 2001); and the exposure of core complexes associated with strike-slip faults within the zone of back-arc extension (Verge, 1993; Bozkurt and Park, 1994), (2) gravitational stretching of the crust initiating extension and graben development (Dewey, 1988; Seyitoğlu and Scott, 1991, 1992; Gautier et al., 1999) and (3) the development of broadly E–W-trending graben systems associated with the westward escape of the Aegean–Anatolian Microplate and the counterclockwise rotation of the Aegean segment of the microplate (McKenzie, 1972, 1978; Tapponier, 1977; Dewey and Şengör, 1979; Şengör, 1979, 1987; Şengör et al., 1985).

Reconstructions based on paleomagnetic data from the southern Aegean region, including central and western Anatolia, suggest that the convergence zone between the African Plate and the Aegean–Anatolian Microplate had a broadly E–W trend in the early Miocene (Morris and Anderson, 1996; Walcott and White, 1998; Kissel et al., 2003; Van Hinsbergen et al., 2007). These studies documented that the western and eastern segments of the Aegean segment of the Aegean–Anatolian Microplate experienced 22–30° clockwise and 19–33° counterclockwise rotations since the middle Miocene, respectively, leading to the present-day morphology of the Hellenic Arc (Fig. 17b). Plate kinematics based on GPS measurements show that the block rotations 4° clockwise in Greece and 5° counterclockwise in Anatolia since the last 4 my (e.g., McClusky et al., 2000; Kreemer and Chamotrooke, 2004).

The present-day tectonic framework of the Aegean Sea is characterized by several NE–SW-striking normal faults bounding basins with similar trend, such as the North Skyros Basin and the North Aegean Trough, and ridges, such as the Mansell Bank, and the North Sporades-Limnos and Euboea-Lesbos Ridges (Fig. 17b; (Exploration, 1989; Mascle and Martin, 1990; Papanikolaou et al., 2002). On the basis of fault-plane solutions of recent earthquakes, Taymaz et al. (1991) suggested that these NE–SW-striking normal faults must have considerable dextral strike-slip motions. In the western Aegean Sea, the NE–SW-striking faults terminate against a series of NW–SE-striking and NE-dipping normal faults, which define the morphology of the eastern shores of many parts of Greece, delimiting the shelf-slope break (Exploration, 1989; Mascle and Martin, 1990; Papanikolaou et al., 2002).

Taymaz et al. (1991) used focal mechanisms of earthquakes constrained by P and SH body wave modeling and by first motions to examine the kinematics of the westward motion of the Aegean–Anatolian Microplate relative to a fixed Eurasian Plate. They showed that the prominent faults in the western Aegean region are mostly normal faults with a NW to WNW strike and with slip vectors directed NNW to NNE. They argued that in the central and eastern Aegean region, distributed right-lateral strike-slip is more prevalent, on faults striking NE to ENE, and with slip vectors directed NE. Taymaz et al. (1991) pointed out that the splays of the North Anatolian Fault enter the Aegean Sea where they define several fault blocks which are elongated parallel with the faults, and that these faults abut the NW-striking normal faults that define the eastern margin of mainland Greece. They argued that the kinematics of the deformation in the Aegean region is controlled by (i) the westward motion of the Aegean–Anatolian Microplate relative to a fixed Eurasian Plate (ii) the collision between northwestern Greece–Albania and the Apulia–Adriatic Platform in the west and (iii) the Hellenic subduction zone in the south. Taymaz et al. (1991) suggested that the Hellenic Arc formed the free edge of the continental shortening allowing the southward roll-back of the subduction zone, and creating the observed N–S extension of the Aegean region. They proposed an eloquent model where the geometry of the deformation resembles a system of broken slats attached to the internally rotating margins (Fig. 17a).

Armijo et al. (1996, 1999) proposed a similar tectonic model for the Aegean region where subduction roll-back and the associated back-arc extension creates E–W and ESE–WNW extension and sinistral shear dominates the eastern regions of the Aegean Sea, whereas E–W to ENE–WSW extension and dextral shear leads to the development of broadly N–S-elongated depressions in the western Aegean Sea. However, Yaltırak (2003) argued that the first-order morphology and the onland geology of western Turkey are at odds with the models proposed by McKenzie (1978), Şengör (1979), Taymaz et al. (1991) and Armijo et al. (1999). He based this

assessment on the presence of normal and transtensional faults in the Aegean Sea and transpressional faults in western Turkey (e.g., Fig. 17a).

In this paper, we use the tectonic architecture of the Bababurnu Basin and the Biga Shelf to propose a variation on the broken-slat model originally proposed by Taymaz et al. (1991). We refer to this as the "rotational wedge model": we envisage the presence of several northwest-oriented asymmetric rotational wedges that control the morpho-tectonic framework of the Aegean region (Fig. 18). In keeping with the broken-slat model of Taymaz et al. (1991), we propose in our rotational wedge model that the NE–SW-striking dextral strike-slip faults splaying off from the North Anatolian Fault system define the boundaries of similarly-trending basins and ridges in the Aegean Sea. These NE–SW-striking faults terminate against NW–SE-striking normal faults bordering the eastern shores of mainland Greece. The rotation wedge model proposed in this study may be similar to fault terminations against the western Transverse Ranges in California (e.g., Luyendyk, 1991; Astiz and Shearer, 2000).

The middle strand of the North Anatolian Fault enters the Aegean Sea near Behramkale in the southern Biga Peninsula. It swings to a northwesterly trend near the southwestern tip of the Biga Peninsula and links with the fault system that defines the northeastern margin of the North Skyros Basin (Figs. 10 and 17b). This NW-striking segment which runs along the southwestern margin of the Biga Shelf is interpreted as a step-over fault. Similar step-over transfer zones are also proposed to occur at various localities along the northern and southern segments of the North Anatolian Fault (e.g., (Papanikolaou et al., 2002; Ustaömer et al., 2008). For example, there are three smaller right-lateral step-over faults in the Saros Basin associated with the northern segment of the North Anatolian Fault (Ustaömer et al., 2008). Similarly, right-lateral step-over faults are proposed for the western portion of the North Aegean Trough, again associated with the northern segment of the North Anatolian Fault (Papanikolaou et al., 2002). The Bababurnu Basin is developed immediately south and southwest of the step-over fault as a pull-apart basin, guided by the development of the step-over fault. We speculate that a splay of the middle strand of the North Anatolian Fault defines the southeastern margin of the offshore pull-apart basin, coinciding with the northwestern margin of Lesvos Island (Fig. 10). The step-over fault connecting the Behramkale Fault to the Biga Fault defines the northwestern boundary of the NE–SW-trending R2 ridge. The northwestern boundary of this ridge and the southeastern boundary of the North Skyros Basin are defined by the Bozcaada Fault (Fig. 17b).

We note that the distance between the strands of the North Anatolian Fault is narrow in the northeastern part of the Aegean Sea, but becomes progressively wider toward the southwest, with each fault block resembling a fan-shaped wedge (Figs. 17b and 18). GPS measurements clearly document a progressive southward rotation and expansion of each wedge (Figs. 1A and 18). A common characteristic of these rotated wedges is the presence of faults with normal dip and dextral strike slip separations as their basin bounding faults, generated by the counterclockwise rotation of the Aegean segment of the Aegean–Anatolian Microplate (Figs. 1 and 17). We further note that there are strong similarities in the morphology and structural architecture, thus the evolutionary mechanism of various basins in the Aegean Sea. For example, the evolution of the Saros and Sporades Basins along the northern strand of the North Anatolian Fault mimics that of the Bababurnu and the North Skyros Basins along the middle strand of the North Anatolian Fault, which in turn mimics the evolution of the South Skyros and North Ikaria Basins along the southern strand of the North Anatolian Fault (Figs. 1 and 18).

The relationship between strike-slip faulting and extensional tectonics throughout the Aegean region was first described by Taymaz et al. (1991) using a broken-slat model (Fig. 17a). However, the onland portion of this model predicts that the orientations of the slats in western Turkey are asymmetric (Fig. 17a; Yaltırak, 2003). Taking into account the southward-directed onland GPS vectors in the area of these slats (Figs. 1A and 18) requires a reinterpretation of the seismotectonics of the Northern Aegean area.

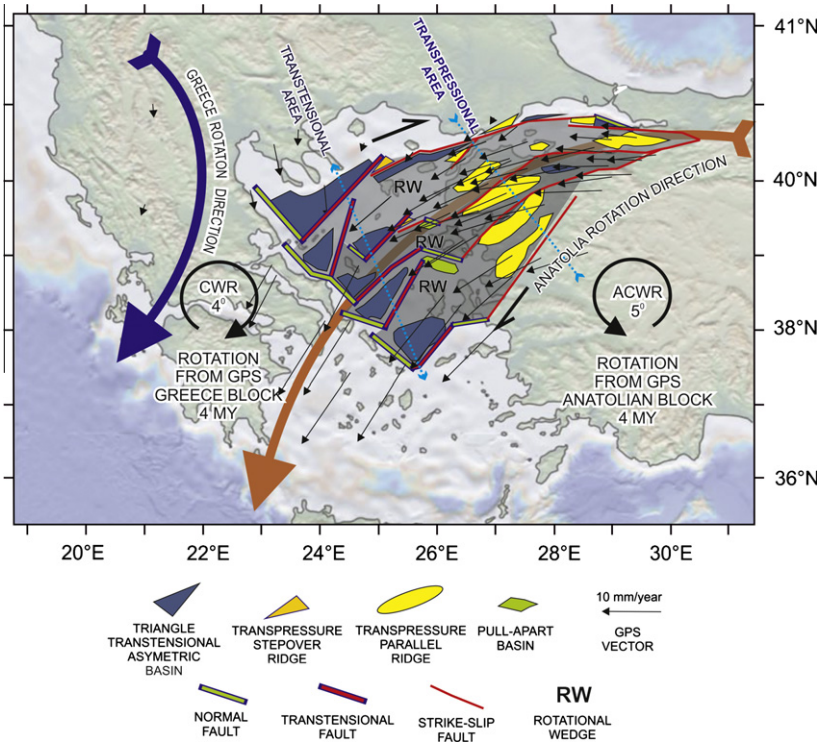

Fig. 18. Aegean rotational wedge model (this study). GPS vectors from Reilinger et al. (2010), Greece and Anatolia rotation degree from GPS vectors for last 4 my. See for simplified fault pattern in Fig. 17B.

Our rotational wedge model (Fig. 18) provides an alternative to the Taymaz et al. (1991) model and better explains the asymmetric slats. Specifically, the NE–SW-striking strike-slip faults which extend west and southwest from Anatolia bound Quaternary marine basins and their intervening ridges in the Aegean Sea (Figs. 17b and 18). There are several such rotational wedges in the Aegean Sea with oblique extensional faults that splay as a fan-shaped geometry from the strands of the North Anatolian Fault (Fig. 18). These large-scale structures are bounded on their western margins by NW–SE-striking extensional faults situated along the eastern coast of Greece (Figs. 17 and 18). Our model shows a compelling geometric similarity to the faults systems of the northern Aegean Sea. In both cases, the major structures are clearly expressed by the morphology of the seafloor (Fig. 17b).

9. Conclusions

Examination of seismic reflection profiles and data from piston cores reveals the following salient conclusions:

- The acoustic basement in the region between the Islands of Limnos, Bozcaada and Lesvos in the northeastern Aegean Sea defines two prominent NE–SW-trending ridges (R1 and R2) and three intervening basins on the shelf (B1, B2 and B3). Basin B1 extends seaward into the deep-water Bababurnu Basin and B3 into the deep-water North Skyros Basin. First-order correlations suggest that these ridges and basins can be linked with similar trending horsts and graben on the Biga Peninsula and northwestern Turkey.
- The Quaternary-Recent tectonic framework of the study area is characterized by two major through-going master faults, referred to as the Bababurnu and Biga Faults. A small pull-apart basin (i.e., the Bababurnu Basin) developed in the southern part of the study area in the Quaternary, controlled by these through-going master faults.
- The middle segment of the North Anatolian Fault is interpreted to extend from Behramkale on land into Edremit Bay, deviating toward the southwest off the Island of Lesvos and continuing farther seaward in a NE–SW direction paralleling the Biga Fault. Two major through-going master faults (Bababurnu and Biga Faults) are interpreted to represent the seaward continuations of the middle segment of the North Anatolian Fault.
- The development of the Bababurnu Basin serves as a model for the evolution of basins in the northern Aegean Sea. We propose that the tectonic framework of the Aegean region is characterized by several asymmetrical rotational wedges. Splays from the dextral North Anatolian Fault zone extend westward into the Aegean Sea as a series of NE–SW-striking strike-slip faults which bound Quaternary marine basins and their intervening ridges in the Aegean Sea. These large-scale structures are bounded on their western margins by NW–SE-striking extensional faults situated along the eastern coast of Greece (Fig. 18).

Acknowledgements

We thank the officers and crew of the R.V. Koca Piri Reis of the Institute of Marine Sciences and Technology, Dokuz Eylül University for their assistance in data acquisition. We acknowledge research and ship-time funds awarded by the Natural Sciences and Engineering Research Council of Canada (NSERC) to Aksu and Hiscott, travel funds from the Dean of Science, Memorial University of Newfoundland, and a special grant from the Vice-President Research, Memorial University of Newfoundland. Yaltırak thanks Jeremy Hall of Memorial University of Newfoundland for partially funding his Post Doctoral Fellowship in 2004–2005 and his Research Fellowship in 2009.

References

Aksu, A.E., Piper, D.J.W., 1983. Progradation of the late quaternary Gediz Delta, Turkey. Marine Geology 54, 1–25.
Aksu, A.E., Piper, D.J.W., Konuk, Y.T., 1987. Late quaternary tectonic and sedimentary history of outer Izmir and Candarli Bays, Western Turkey. Marine Geology 76, 89–104.
Aksu, A.E., Calon, T.J., Piper, D.J.W., Turgut, S., İzdar, E., 1992a. Architecture of late orogenic quaternary basins in northeastern mediterranean-sea. Tectonophysics 210, 191–213.
Aksu, A.E., Uluğ, A., Piper, D.J.W., Konuk, Y.T., Turgut, S., 1992b. Quaternary sedimentary history of Adana, Cilicia and Iskenderun Basins – northeast mediterranean-sea. Marine Geology 104, 55–71.
Aksu, A.E., Yaşar, D., Mudie, P.J., Gillespie, H., 1995. Late glacial-Holocene paleoclimatic and paleoceanographic evolution of the Aegean Sea: micropaleontological and stable isotopic evidence. Mar. Micropaleontol. 25, 1–28.
Aksu, A.E., Hall, J., Yaltırak, C., 2009. Miocene-recent evolution of Anaximander Mountains and Finike Basin at the junction of Hellenic and Cyprus Arcs, Eastern Mediterranean. Marine Geology 258, 24–47.
Altunkaynak, S., Yılmaz, Y., 1998. The Mount Kozak magmatic complex, Western Anatolia. Journal of Volcanology and Geothermal Research 85, 211–231.
Armijo, R., Meyer, B., King, G.C.P., Rigo, A., Papanastassiou, D., 1996. Quaternary evolution of the Corinth Rift and its implications for the late cenozoic evolution of the Aegean. Geophysical Journal International 126, 11–53.
Armijo, R., Meyer, B., Hubert-Ferrari, A., Barka, A.A., 1999. Westward propagation of North Anatolian Fault into the Northern Agean: timing and kinematics. Geol 27, 267–270.
Astiz, L., Shearer, P.M., 2000. Earthquake locations in the inner continental borderland, offshore Southern California. Bulletin of the Seismological Society of America 90, 425–449.
Barka, A.A., Kadinsky-Cade, K., 1988. Strike-slip fault geometry in Turkey and its influence on earthquake activity. Tectonics 7, 663–684.
Biju-Duval, B., Dercourt, J., Le Pichon, X., Apostolescu, V., 1977. Evolution from Tethys to Mediterranean Basins (in Histoire Structurale Des Bassins Mediterraneens, Geologie Et Geophysique Marines. Structural History of Mediterranean Basins, Geology and Marine Geophysics, Cousteau). Rapports et Proces Verbaux des Reunions, Commission Internationale pour l'Exploration Scientifique de la Mer Mediterranee 24, 51–52.
Bintanja, R., van de Wal, R.S.W., Oerlemans, J., 2005. Modelled atmospheric temperatures and global sea levels over the past million years. Nature 437, 125–128.
Bozkurt, E., Park, R.G., 1994. Southern Menderes Massif – an incipient metamorphic core complex in Western Anatolia, Turkey. Journal of the Geological Society 151, 213–216.
Bozkurt, E., Oberhansli, R., 2001. Menderes massif (Western Turkey): structural, metamorphic and magmatic evolution – a synthesis. International Journal of Earth Sciences 89, 679–708.
Boztepe-Güney, A., Yılmaz, Y., Demirbağ, E., Ecevitoğlu, B., Arzuman, S., Kusçu, I., 2001. Reflection seismic study across the continental shelf of Baba Burnu Promontory of Biga Peninsula, Northwest Turkey. Marine Geology 176, 75–85.
Caputo, R., 2007. Sea-level curves: perplexities of an end-user in morphotectonic applications. Global and Planetary Change 57, 417–423.
Chappell, J., Shackleton, N.J., 1986. Oxygen isotopes and sea-level. Nature 324, 137–140.
Dewey, J.F., Şengör, A.M.C., 1979. Aegean and surrounding regions – complex multiplate and continuum tectonics in a convergent zone. Geological Society of America Bulletin 90, 84–92.
Dewey, J.F., 1988. Extensional collapse of orogens. Tectonics 7, 1123–1139.
Dooley, T., McClay, K., 1997. Analog modeling of pull-apart basins. Aapg Bulletin-American Association of Petroleum Geologists 81, 1804–1826.
Edwards, R.L., Gallup, C.D., Cheng, H., 2003. Uranium-series dating of marine and lacustrine carbonates. In: Bourdon, B., Henderson, G.M., Lundstrom, C.C., Turner, S.P. (Eds.), Uranium-series Geochemistry. Mineralogical Society of America, Washington, DC, pp. 363–405.
Ericson, A.J., 1978. Leg 42A Physical properties data. In: Hsü, K., Montadert, L., et al. (Eds.), Initial Reports of the Deep Sea Drilling Project, vol. 42, Part 1. U.S. Government Printing Office, Washington, pp. 1199–1206.
Eriksen, U., Friedrich, W.L., Buchardt, B., Tauber, H., Thomson, M.S., 1990. The Stronghyle Caldera: geological, paleontological and stable isotope evidence from radiocarbondated stromatolites from Santorini. In: Hardy, D.A., Keller, J., Galanopoulos, V.P., Flemming, N.C., Druitt, T.H. (Eds.), Thera and the Aegean World III. Santorini, Greece, pp. 139–150.
Gautier, P., Brun, J.P., Moriceau, R., Sokoutis, D., Martinod, J., Jolivet, L., 1999. Timing, kinematics and cause of Aegean extension: a scenario based on a comparison with simple analogue experiments. Tectonophysics 315, 31–72.
Genç, Ş.C., 1998. Evolution of the Bayramic magmatic complex, northwestern Anatolia. Journal of Volcanology and Geothermal Research 85, 233–249.
Helland-Hansen, W., Martinsen, O.J., 1996. Shoreline trajectories and sequences: description of variable depositional-dip scenarios. Journal of Sedimentary Research 66, Pg 671 1170-1170.
Hsü, K.J., Montadert, L., Bernoulli, D., Cita, M.B., Erickson, A.J., Garrison, R.E., Kidd, R.B., Melieres, F., Muller, C., Wright, R., 1977. History of the Mediterranean Salinity Crisis.

Igme, 1989. Seismotectonic Map of Greece with Seismological Data. Institute of Geology and Mineral Exploration, Athens.
Imbrie, J., Hays, J.D., Martinson, D.G., Mc Intyre, A., Mix, A.C., Morley, J.J., Pisias, N.G., Prell, W.L., Shackleton, N.J., 1984. The Orbital Theory of Pleistocene Climate: Support from Revised Chronology of the Marine Δ18° Record, vol. 126. Reidel Publishing Company, Boston, pp. 269–305.
Ioc, 1981. International Bathymetric Chart of the Mediterranean. A Regional Ocean Mapping Project of the Intergovernmental Oceanographic Commission I.O. Commission, Department of Navigation and Oceanography Soviet Union, Moscow, 10 sheets.
İşler, E.B., Aksu, A.E., Yaltırak, C., Hiscott, R.N., 2008. Seismic stratigraphy and quaternary sedimentary history of the Northeast Aegean Sea. Marine Geology 254, 1–17.
Kahle, H.G., Straub, C., Reilinger, R., McClusky, S., King, R., Hurst, K., Veis, G., Kastens, K., Cross, P., 1998. The strain rate field in the eastern mediterranean region, estimated by repeated Gps measurements. Tectonophysics 294, 237–252.
Kiratzi, A.A., Wagner, G.S., Langston, C.A., 1991. Source parameters of some large earthquakes in northern Aegean determined by body wave-form inversion. Pure and Applied Geophysics 135, 515–527.
Kissel, C., Laj, C., Poisson, A., Görür, N., 2003. Paleomagnetic reconstruction of the cenozoic evolution of the eastern mediterranean. Tectonophysics 362, 199–217.
Kreemer, C., Chamotrooke, N., 2004. Contemporary kinematics of the Southern Aegean and the mediterranean ridge. Geophysical Journal International 157, 1377–1392.
Lalechos, N. and Savoyat, E., 1977. La Sédimentation Néogène Dans Le Fossé Nord Egéen. The VI Colloquium on the Geology of the Aegean Region, vol. 2, Greece, Athene, pp. 591–603.
Le Pichon, X., Angelier, J., 1979. Hellenic arc and trench system – key to the neotectonic evolution of the eastern mediterranean area. Tectonophysics 60, 1–42.
Le Pichon, X., Angelier, J., 1981. The Agean Sea. Philosophical Transactions of the Royal Society of London 300, 357–372.
Luyendyk, B.P., 1991. A model for Neogene crustal rotations, transtention and transpression in southern California. Geol 103, 1528–1536.
Lykousis, V., 2009. Sea-level changes and shelf break prograding sequences during the last 400 Ka in the Aegean Margins: subsidence rates and palaeogeographic implications. Continental Shelf Research 29, 2037–2044.
Mascle, J., Martin, L., 1990. Shallow structure and recent evolution of the Aegean Sea – a synthesis based on continuous reflection profiles. Marine Geology 94, 271–299.
McClusky, S., Balassanian, S., Barka, A., Demir, C., Ergintav, S., Georgiev, I., Gurkan, O., Hamburger, M., Hurst, K., Kahle, H., Kastens, K., Kekelidze, G., King, R., Kotzev, V., Lenk, O., Mahmoud, S., Mishin, A., Nadariya, M., Ouzounis, A., Paradissis, D., Peter, Y., Prilepin, M., Reilinger, R., Sanli, I., Seeger, H., Tealeb, A., Toksoz, M.N., Veis, G., 2000. Global positioning system constraints on plate kinematics and dynamics in the eastern mediterranean and Caucasus. Journal of Geophysical Research-Solid Earth 105, 5695–5719.
McKenzie, D., 1972. Active tectonic of the mediterranean region. The Geophysical Journal of the Royal Astronomical Society 30, 109–185.
McKenzie, D., 1978. Active tectonics of Alpine-Himalayan Belt – Aegean Sea and surrounding regions. Geophysical Journal of the Royal Astronomical Society, 55, 217-and.
McKenzie, D., Yılmaz, Y., 1991. Deformation and volcanism in western Turkey and the Aegean. Bulletin of the Istanbul Technical University 44, 345–373.
Meade, B.J., Hager, B.H., McClusky, S.C., Reilinger, R.E., Ergintav, S., 2002. Estimates of seismic potential in the Marmara sea region from block models of secular deformation constrained by global positioning system. Bulletin of the Seismological Society of America 92, 208–215.
Mitchum, R.M., Vail, P.R., Thompson, S.R., 1977. Seismic stratigraphy and global changes of sea level: Part 2. The depositional sequence as a basic unit for stratigraphic analysis: Section 2. Application of seismic reflection configuration to stratigraphic interpretation. American Association of Petroleum Geologists Speical Memoir 26, 53–62.
Morris, A., Anderson, M., 1996. First palaeomagnetic results from the Cycladic Massif, Greece, and their implications for Miocene extension directions and tectonic models in the Aegean. Earth and Planetary Science Letters 142, 397–408.
Öztürk, K., Yaltırak, C., Alpar, B., 2009. The relationship between the tectonic setting of the Lake Iznik Basin and the Middle strand of the North Anatolian fault. Turkish Journal of Earth Sciences 18, 209–224.
Papadimitriou, E.E., Sykes, L.R., 2001. Evolution of the stress field in the Northern Aegean Sea (Greece). Geophysical Journal International 146, 747–759.
Papanikolaou, D., Alexandri, M., Nomikou, P., Ballas, D., 2002. Morphotectonic structure of the western part of the north Aegean basin based on swath bathymetry. Marine Geology 190, 465–492.
Papanikolaou, I.D., Papanikolaou, D.I., 2007. Seismic hazard scenarios from the longest geologically constrained active fault of the Aegean. Quaternary International 171–72, 31–44.
Papazachos, B.C., Papadimitriou, E.E., Kiratzi, A.A., Papazachos, C.B., Louvari, E.K., 1998. Fault plane solutions in the Aegean Sea and the surrounding area and their tectonic implication. Bolletino di Geofisica Teorica ed Applicata 39, 199–218.
Pe-Piper, G., Piper, D.J.W., 2001. Late cenozoic, post-collisional Aegean igneous rocks: Nd, Pb and Sr isotopic constraints on petrogenetic and tectonic models. Geological Magazine 138, 653–668.
Piper, D.J.W., Perissoratis, C., 1991. Late quaternary sedimentation on the North Aegean Continental-Margin, Greece. American Association of Petroleum Geologists 75, 46–61.
Reilinger, R., McClusky, S., Oral, M., King, R., Toksöz, M., Barka, A., Kınık, I., Lenk, O., Sanlı, I., 1997. Global positioning system measurements of present-day crustal movements in the Arabia–Africa–Eurasia plate collision zone. Journal of Geophysical Research 102, 9983–9999.
Reilinger, R., McClusky, S.C., Paradissis, D., Ergintav, S., Vernant, P., 2010. Geodetic constraints on the tectonic evolution of the Aegean region and strain accumulation along the Hellenic subduction zone. Tectonophysics 488, 22–30.
Ryan, W.B.F., Carbotte, S.M., Coplan, J.O., O'Hara, S., Melkonian, A., Arko, R., Weissel, R.A., Ferrini, V., Goodwillie, A., Nitsche, F., Bonczkowski, J., Zemsky, R., 2009. Global multi-resolution topography synthesis. Geochemistry Geophysics Geosystems, 10.
Saatçılar, R., Ergintav, S., Demirbağ, E., İnan, S., 1999. Character of active faulting in the North Aegean Sea. Marine Geology 160, 339–353.
Sakınç, M., Yaltırak, C., 2005. Messinian crisis: what happened around the Northeastern Aegean? Marine Geology 221, 423–436.
Seyitoğlu, G., Scott, B., 1991. Late Cenozoic crustal extension and basin formation in West Turkey. Geological Magazine 128, 155–166.
Seyitoğlu, G., Scott, B.C., 1992. Late Cenozoic volcanic evolution of the northeastern Aegean Region. Journal of Volcanology and Geothermal Research 54, 157–176.
Shipboard Scientific Staff, 1978. In: Ross, D.A., Neprochnov, Y.P., et al. (Eds.), Initial Reports of the Deep Sea Drilling Project, vol. 42, Part 2. U.S. Government Printing Office, Washington, pp. 1131–1137.
Siyako, M., Bürkan, A.K., Okay, A.I., 1989. Tertiary geology and hydrocarbon potential of the Biga and Gelibolu Peninsulas. Bulletin of Turkish Association Petroleum Geologists 1, 183–199.
Skene, K.I., Piper, D.J.W., Aksu, A.E., Syvitski, J.P.M., 1998. Evaluation of the global oxygen isotope curve as a proxy for quaternary sea level by modeling of delta progradation. Journal of Sedimentary Research 68, 1077–1092.
Şengör, A.M.C., 1979. The north anatolian transform fault; its age, offset and tectonic significance. Journal of the Geological Society of London 136, 269–282.
Şengör, A.M.C., Görür, N., Şaroğlu, F., 1985. Strike-slip faulting and related basin formation in zones of tectonic escape: Turkey as a case study. In: Biddle, K.T., Christie-Blick, N. (Eds.), Strike-Slip Deformation, Basin Formation, and Sedimentation, Soc. Econ. Paleontol. Spec. Publ., 37, pp. 227–264.
Şengör, A.M.C., 1987. Cross-faults and differential stretching of hanging walls in regions of low-angle normal faulting; examples from Western Turkey. In: Coward, M.P., Dewey, J.F., Hancock, P.L. (Eds.), Continental Extensional Tectonics. Geological Society Special Publications, London, pp. 575–589, vol. 28.
Şengör, A.M.C., Tüysüz, O., İmren, C., Sakınç, M., Eyidoğan, H., Gorur, N., Le Pichon, X., Rangin, C., 2005. The north Anatolian fault: a new look. Annual Review of Earth and Planetary Sciences 33, 37–112.
Tapponier, P., 1977. Evolution Téctonique Du Systeme Alpin En Méditerrannée: Poinconnement Et Écrasement Rigide-Plastique. Bulletin de la Société Géologique de France 19, 437–460.
Taymaz, T., Jackson, J., McKenzie, D., 1991. Active tectonics of the north and central Aegean Sea. Geophysical Journal International 106, 433–490.
Ustaömer, T., Gokaşan, E., Tur, H., Görum, T., Batuk, F.G., Kalafat, D., Alp, H., Ecevitoğlu, B., Birkan, H., 2008. Faulting, mass-wasting and deposition in an active dextral shear zone, the Gulf of Saros and the Ne Aegean Sea, Nw Turkey. Geo-Marine Letters 28, 171–193.
Van Hinsbergen, D.J.J., Krijgsman, W., Langereis, C.G., Cornee, J.J., Duermeijer, C.E., Van Vugt, N., 2007. Discrete plio-pleistocene phases of tilting and counterclockwise rotation in the Southeastern Aegean Arc (Rhodos, Greece): early pliocene formation of the South Aegean left-lateral strike-slip system. Journal of the Geological Society 164, 1133–1144.
Verge, N.J., 1993. Oligo-Miocene Orogenic Collapse Tectonics in Western Anatolia and the Extensional Exhumation of the Menderes Massif Metamorphic-Core-Complex. In: Seranne, M., Malavieille, J. (Eds.), Late Orogenic Extension in Mountain Belts, vol. 219. Documents des Bureau de Recherches Géologique et Minières France, pp. 202.
Walcott, C.R., White, S.H., 1998. Constraints on the kinematics of post-orogenic extension imposed by stretching lineations in the Aegean Region. Tectonophysics 298, 155–175.
Yaltırak, C., 1995. Tectonic mechanism controlling the plio-quaternary sedimentation in the Gelibolu Peninsula. Jeofizik 9, 104–106.
Yaltırak, C., Alpar, B., Yüce, H., 1998. Tectonic elements controlling the evolution of the Gulf of Saros (Northeastern Aegean Sea, Turkey). Tectonophysics, 300, 227-+.
Yaltırak, C., Alpar, B., Sakınc, M., Yüce, H., 2000a. Origin of the strait of Canakkale (Dardanelles): regional tectonics and the mediterranean-Marmara incursion. Marine Geology 164, 139–156.
Yaltırak, C., Sakınç, M., Oktay, F.Y., 2000b. Westward propagation of north Anatolian Fault into the Northern Aegean: timing and kinematics, comment. Geology 28, 187–189.
Yaltırak, C., 2002. Tectonic evolution of the Marmara Sea and its surroundings. Marine Geology 190, 493–529.
Yaltırak, C., Alpar, B., 2002a. Evolution of the middle strand of north Anatolian fault and shallow seismic investigation of the southeastern Marmara Sea (Gemlik Bay). Marine Geology 190, 307–327.
Yaltırak, C., Alpar, B., 2002b. Kinematics and evolution of the northern branch of the North Anatolian Fault (Ganos Fault) between the Sea of Marmara and the Gulf of Saros. Marine Geology 190, 351–366.
Yaltırak, C., 2003. Geodynamic Evolution of the Gulf of Edremit and Northern Area. İstanbul Techincal University, İstanbul.
Yılmaz, Y., Karacık, Z., 2001. Geology of the northern side of the Gulf of Edremit and its tectonic significance for the development of the Aegean Grabens. Geodinamica Acta 14, 31–43.